2009-01-01

RC Structures Strengthened with Mechanically Fastened FRP Systems

Annalisa Napoli
University of Miami, a.napoli@umiami.edu

UNIVERSITY OF MIAMI

RC STRUCTURES STRENGTHENED WITH MECHANICALLY FASTENED FRP SYSTEMS

By

Annalisa Napoli

A THESIS

Submitted to the Faculty
of the University of Miami
in partial fulfillment of the requirements for
the degree of Master of Science

Coral Gables, Florida

December 2008

UNIVERSITY OF MIAMI

A thesis submitted in partial fulfillment of
the requirements for the degree of
Master of Science

RC STRUCTURES STRENGTHENED WITH MECHANICALLY FASTENED FRP SYSTEMS

Annalisa Napoli

Approved:

_____ Antonio Nanni, Ph.D. Professor and Chair of Civil, Architectural and Environmental Engineering Department	_____ Terri A. Scandura, Ph.D. Dean of the Graduate School
_____ Fabio Matta, Ph.D. Research Assistant Professor of Civil, Architectural and Environmental Engineering	_____ Brian Metrovich, Ph.D. Assistant Professor of Civil, Architectural and Environmental Engineering
_____ Roberto Realfonzo, Ph.D. Associate Professor of Civil and Environmental Engineering University of Salerno, Italy	

NAPOLI, ANNALISA (M.S., Civil Engineering)

RC Structures Strengthened with Mechanically Fastened FRP Systems (December 2008)

Abstract of a thesis at the University of Miami.

Thesis supervised by Professor Antonio Nanni.
No. of pages in text. (67)

Recently, the use of Mechanically Fastened Fiber-Reinforced Polymer (MF-FRP) systems has emerged as a viable means for flexural strengthening of reinforced concrete members. The technique is suitable for emergency repairs where constructability and speed of installation are critical requirements. The MF-FRP system consists of pre-cured FRP laminates with enhanced longitudinal bearing strength that are attached to the concrete substrate by means of mechanical steel anchors. This research project presents an experimental investigation comprising a series of flexural tests on scaled one-way RC slabs. The test matrix includes MF-FRP strengthened specimens, a counterpart with the externally bonded (EB) FRP reinforcement, and a control specimen. The effects of fastener layout and laminate length on strength increase and failure mode were studied. It is shown that with proper selection of fastener layout the MF-FRP system results in a significant deformability and strength increase, where the latter is comparable to that attained using EB-FRP sheets. Specific gaps on the existing analytical procedures for flexural strengthening with MF-FRP systems are finally discussed.

To
my uncle Lucio and my aunt Fulvia

ACKNOWLEDGMENTS

First, I would like to thank my advisor, Dr. Antonio Nanni, for his guidance throughout the duration of this project. His vision and direction made this a tremendous learning experience.

I also would like to express my appreciation to my overseas advisor, Dr. Roberto Realfonzo, for providing me his advice, knowledge and support during this wonderful experience at the University of Miami: my being here was made possible by Dr. Realfonzo and the University of Salerno.

Special thanks to Dr. Matta for the support and precious advice he provided me during the duration of this project.

I also wish to express my appreciation to Dr. Metrovich for his advice, support and brilliant M.S. courses offered at the University of Miami.

I would like to thank the NSF I/UCRC "Repair of Buildings and Bridges with Composites" (RB^2C) for funding this research and Strongwell Inc. for providing all of the composite materials used during the testing.

I would like to recognize the graduate and undergraduate students of the Civil, Architectural, and Environmental Engineering Department for providing support throughout the project. Special thanks to Derek Schesser for helping me in the lab.

The biggest hug goes to my family and my boyfriend, for their love and support throughout the duration of my studies.

Finally, I will never forget the love provided by my "American parents," Leslie and Sondra Space. Without their immeasurable support, all this would not have been possible.

TABLE OF CONTENTS

LIST OF FIGURES

Page

LIST OF TABLES

Page

CHAPTER 1

INTRODUCTION

1.1 GENERAL

Over the past decade, the demand for strengthening existing reinforced concrete (RC) structures is significantly increased. Nowadays, there is a pressing need for upgrading the bridge infrastructure built between the 1930 and 1970 in the United States, predominantly due to maintenance and construction-related deficiencies, materials deterioration and demand for higher permissible overloads.

Recently, the use of fiber-reinforced polymer (FRP) materials for the repairing and strengthening of structures has emerged as one of the most promising technologies for structural application and is expected to increase significantly in future. Applications of FRP composites in civil and infrastructure engineering include both internal and external reinforcement for concrete and structural elements (Bakis et al. 2002; Teng et al. 2002).

Most current work related to the flexural strengthening of RC structures with FRP materials entails the use of FRP laminates adhesively bonded to the concrete substrate (Triantafillou and Matthys 2001) or FRP rods embedded into grooves cut in the concrete cover (De Lorenzis and Nanni 2001; De Lorenzis and Teng 2007). The feasibility of these two techniques, often referred to as Externally Bonded (EB) FRP and Near-Surface Mounted (NSM) FRP systems, respectively, is also evidenced by development of design and construction guidelines recommended by the American Concrete Institute (ACI 2008a). However, part of the effectiveness of current strengthening systems is offset by the need of time-consuming and labor-intensive operations to provide adequate compatibility between FRP laminate and concrete substrate.

In the case of EB-FRP systems, prior to applying the FRP laminate, the concrete substrate needs to be sandblasted, cleaned and smoothened, which may delays the immediate availability of the strengthened structure (Stallings and Tedesco 2000; Hag-Elsafi et al. 2001). Furthermore, the bonded method is further constrained for immediate use by the curing time of the polymeric adhesive, which is typically up to seven days. In addition, since FRP bonded systems are susceptible to brittle failures of the strengthened member by laminate debonding, mechanical anchorages may be used at the strip ends (Spadea et al. 1998). In case of NSM-FRP systems, although the amount of site installation work may be comparable to the EB-FRP method, concerns related to constructability such as the possibility of damaging the existing steel reinforcing bars may still affect the feasibility of this technique.

Recently, the use of Mechanically Fastened (MF) FRP systems has emerged as a viable means for flexural strengthening of RC members (Lamanna 2002; Lamanna et al. 2001; Lamanna et al. 2004). The technique is suitable for emergency repairs where constructability and speed of installation are critical requirements. In fact, unlike the other two methods discussed, the MF-FRP system requires conventional hand-tools and workmanship, entails minimal surface preparation and enables the immediate use of the strengthened structure. The viability of this technology is corroborated by the increasing number of field applications, often involving civil and military bridge structures (Arora 2003; Rizzo 2005; Bank et al. 2003). MF-FRP systems are also being studied for increasing the flexural capacity of timber members (Dempsey and Scott, 2006).

The MF-FRP system covered in this thesis consists of pre-cured FRP laminates with enhanced longitudinal bearing strength that are attached to the concrete substrate by means of mechanical steel anchors.

Considerable research has been performed to characterize materials and strength properties of FRP laminate/steel fastener connection (Lamanna 2002; Rizzo 2005; Rizzo et al. 2005a). Experimental tests have been carried out on rectangular members as well as on RC T-beams (Lamanna et al. 2004) in order to investigate structural performance.

More work is needed to quantitatively characterize relevant parameters affecting the response of the connection concrete-fastener-FRP laminate, such as fastener typology, fastener layout and length of FRP laminate, to establish analytical tools, and to eventually develop design guidelines.

This research project presents an experimental investigation comprising a series of flexural tests on scaled one-way RC slabs. The test matrix includes MF-FRP strengthened specimens, a counterpart with externally bonded FRP reinforcement, and an unstrengthened (control) specimen. The effects of fastener layout and laminate length on strength increase and failure mode were studied. It is shown that with appropriate selection of fastener layout the MF-FRP system results in a significant deformability and strength increase, where the latter is comparable to that attained using EB-FRP sheets. Specific gaps on the existing analytical procedures for flexural strengthening with MF-FRP systems are finally discussed.

1.2 SIGNIFICANCE

Constructability and emergency repair are the key factors for strengthening RC members with MF-FRP laminate. However, the implementation of the technology is still

limited compared with other methods of flexural strengthening such as EB-FRP and NSM-FRP systems. Knowledge gaps result in the incomplete understanding of parameters affecting the performance of the connection concrete-fastener-FRP laminate and in the unavailability of efficient design procedures.

Concerns are also related to the occurrence of brittle failure modes for members strengthened with the MF-FRP system if appropriate selection of fastener typology, fastener layout and minimum edge distances of the fasteners is not addressed. Also, cost-effectiveness requirements call for analytical procedures for flexural strengthening with MF-FRP laminates that optimize the design with respect to the amount of composite materials used, as well as installation work.

The research project presented in this thesis preliminarly addresses these gaps investigating the influence of relevant parameters such as fastener layout and length of reinforcing FRP laminate on the structural efficiency of the MF-FRP system. In addition, issues raised by the use of existing design procedures are discussed and recommendations for future work are made.

1.3 OBJECTIVES

The objectives of the research project reported in this thesis are as follows:

a) investigate the effectiveness of using MF-FRP laminates for flexural strengthening of RC members compared with the EB-FRP laminates;

b) study the influence of fastener layout and length of reinforcing FRP laminate on the structural performance of the MF-FRP system;

c) investigate the influence of fasteners spacing in increasing the deformability of members strengthened with MF-FRP laminates;

d) verify the efficiency of existing design procedures in predicting flexural response.

1.4 SCOPE OF RESEARCH

The scope of work for the research stated is as follows:

1. **Background investigation.** An accurate study on the existing knowledge of MF-FRP systems was required in order to understand the critical aspects related to the use of this technology. Such investigation primarily included: FRP laminate and fastener types that have been studied for MF-FRP applications; behavior of FRP-fastener-concrete connection; analysis of the existing design procedures for predicting the flexural capacity of RC members strengthened with MF-FRP laminates.

2. Experimental program. The understanding of critical issues raised by the use of MF-FRP systems was the key for the definition of the test plan. The strength models available in the technical literature were used for design of specimens in order to investigate the agreement between experimental results and analytical predictions. Understanding of possible failure modes of the MF-FRP connection was the critical issue for the selection of limiting strains for FRP laminate. Appropriate selection of fastener layouts and length of reinforcing FRP laminate was needed in order to investigate the capability of preventing undesired brittle failure of the MF connection and increasing the deformability of the system. The test matrix included four MF-FRP strengthened specimens, one counterpart with an externally bonded FRP sheet, and one control specimen.

3. Testing of scaled one-way RC slabs. Testing was carried out at the Structural Lab of the Department of Civil, Architectural and Environmental Engineering at the University of Miami, Coral Gables, Florida. The specimens were tested under load

control in four-point bending using a 120 kip (533 kN) hydraulic jack. Data collected included applied load, displacements, strains in the concrete, internal steel reinforcement and FRP laminate.

4. Analysis of test results. Comparisons in terms of strength and deformability between the MF-FRP strengthened slabs and the control specimen, as well as the EB-FRP strengthened specimen, were investigated. The overall performance of slabs strengthened with MF-FRP laminates was shown to be a function of FRP laminate utilization, or the ability of fastener pattern to transfer tensile forces into the FRP laminate. The analysis of strain distribution in the FRP and steel was relevant to the qualitative characterization of the slip occurring between the FRP laminate and concrete substrate. The comparison between the experimental behavior and that assumed in existing models prompted the existence of conceptual limitations related to the use of such models.

CHAPTER 2

LITERATURE REVIEW

2.1 OVERVIEW

This chapter presents an overview of existing knowledge on MF-FRP system for the flexural strengthening of RC members. The literature review examines relevant aspects of this technology in terms of materials used, installation procedures, behavior of MF-FRP connections, and design procedures. The purpose of this review was to identify some of the knowledge gaps that the study presented in this thesis attempted to address.

2.2 EXISTING KNOWLEDGE ON MF – FRP SYSTEM

2.2.1 FRP laminate

Unidirectional pultruded laminates currently used to be adhesively bonded onto the concrete surface are not suitable to be mechanically attached with steel anchors. These laminates are designed to have high modulus and strength in the longitudinal direction and low mechanical properties in the transverse direction of the laminate. Consequently, unless reinforcing fibers in the transverse direction of the laminate are inserted to provide adequate bearing strength, the orthotropic nature of the material causes the splitting failure of the laminate (Figure 2.1) when a fastener is driven through it (Lamanna 2002).

Figure 2.1 – Splitting Failure for existing FRP Laminates (Lamanna 2002)

Precured laminates commercially available for strengthening with MF-FRP systems consist of a glass and carbon hybrid pultruded strip embebbed in a vinyl ester resin (Figure 2.2). The one shown has thickness and width of 0.125 in (3.175 mm) and 4 in (101.6 mm), respectively; the 4 in width is a suitable size for handling in the field. Continuous glass fiber strand mats are used to provide transverse and bearing strength, while 16-113 yield E-glass roving and 40-48k standard modulus carbon tows are utilized to provide longitudinal strength and stiffness. Table 2.1 summarizes the properties of the constituent materials (Arora 2003).

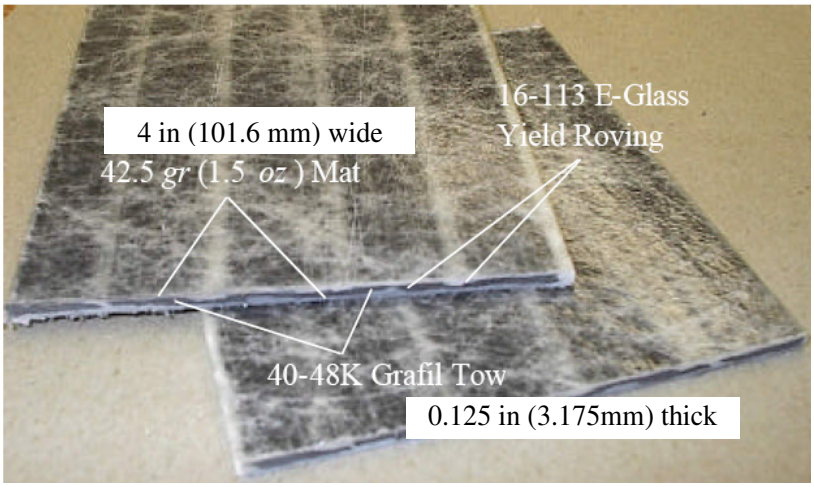

Figure 2.2 – Sample of laminate available for the MF-FRP system

Results on mechanical characterization of the FRP laminate in the longitudinal and transverse direction are reported elsewhere (Arora 2003; Rizzo 2005; Rizzo et al. 2005a); relevant considerations are summarized herein.

In the longitudinal direction, the behavior of the laminate under tensile load is linear elastic up to failure. Figure 2.3 shows the typical failure observed during the tests; Table

2.2 reports the average values of mechanical properties in the longitudinal direction obtained by Arora (2003) and by Rizzo (2005).

Table 2.1 – Properties of the components of the MF-FRP Laminate (Arora 2003)

Component	Tensile Elastic Modulus*	Cross Sectional Area	Thickness**	Ultimate Tensile Strength
	ksi (GPa)	in^2 (mm^2)	in (mm)	ksi (MPa)
16-113 Yield E-glass Roving	10500 (72.4)	0.00268 (1.73)	-	500 (3448)
40-48K Grafil Standard Modulus Carbon Tows	34000 (234.5)	0.002756 (1.778)	-	600 (4137)
1.5 oz Continuous Strand Mat	1000 (6.90)	-	0.029 (0.737)	50 (345)
Vinyl Ester Resin	490 (3.38)	-	-	11.8 (81.4)

*Obtained from manufactures data
** Mat thickness based on 80 psi (552 kPa)

Figure 2.3 – Typical failure under tensile test in longitudinal direction (Arora, 2002)

Open hole tensile tests in longitudinal direction evidenced that the presence of a hole in a generic position along the width of the laminate does not significantly influence the mechanical properties. As a result, the stress on the net area, the elastic modulus and the

strain at failure can be assumed to be equal to the corresponding values found for full size specimens without holes (Rizzo 2005); values lightly lower are indicated by Arora (2003), although based on a limited number of tests performed on coupons having all the same geometry. Table 2.3 reports the average values of mechanical properties found by the authors; Figure 2.4 depicts the typical failure observed during such tests.

Table 2.2 – Results from tensile tests in longitudinal direction

Tests	Failure Stress (ksi)	Modulus of Elasticity (ksi)
Arora (2003)	122.4±11.2	8892±765
Rizzo (2005)	136±16	9509±853

Table 2.3 – Results from open hole tensile tests in longitudinal direction

Tests	Failure Stress (ksi)	Modulus of Elasticity (ksi)
Arora (2003)	639.6±48.6	8892±765
Rizzo (2005)	898±17	10177±562

(1 ksi = 6.895 MPa)

Figure 2.4 – Typical failure for open hole tension tests (Arora 2003)

Bearing tests in the longitudinal direction of the laminate were performed in presence of one or two holes by varying the hole size and the distance from the free edge; no clamping pressure was applied on the contact area pin-FRP material (Table 2.4). The maximum bearing strength does not depend on the pin size and the distance between the hole center and the free edge in the direction normal to the applied load; however a

minimum edge distance of 25 mm is required in the longitudinal direction to exploit the full bearing capacity of the material. The bearing failure has been shown to occur through buckling and brushlike failure with consequent delamination of the outer layers in the material away from the contact area, and elongation of the hole (Figure 2.5).

Table 2.4 – Typical bearing failure observed

Tests	No. of holes	Bearing strength (ksi)
Arora (2003)	1	34.0
Rizzo (2005)	1	34.1±2.5
	2	31.0±2.3

(1 ksi = 6.895 MPa)

Figure 2.5 – Typical bearing failure observed (Arora, 2003)

Tensile tests performed in the transverse direction showed that the stress-strain behavior of the laminate is not linear and does not depend on the material size; the stress-strain curve is similar to a parabola with modulus at the origin equal to 7151 MPa (1037 ksi). The average values of the stress and strain at failure, based on coupons having different widths, are equal to 65.6 MPa (9.6 ksi) and 13498 με, respectively (Rizzo, 2005).

Results from bearing tests performed in the transverse direction of unconstrained material showed that the bearing strength does not depend on the size of the hole but only on the end distance. Both tension failure and bearing failure thus depend on the ratio w/ϕ (= width of the laminate /diameter of the hole). Nevertheless, bearing failure in the

transverse direction is different from that observed in the longitudinal direction, due to the particular stable configuration that the carbon fibers adopt by creating a natural bend in the contact area against the pin, which increases the capacity until the final secondary net-tension failure (Rizzo 2005). The maximum bearing stress in transverse direction was estimated to be equal on average 160.1 MPa (23.2 ksi).

2.2.2 Anchors

Fastener types that have been investigated for the MF FRP systems include: power-actuated fasteners (PAF), wedge bolts and wedge anchors (Figure 2.6). The PAF system consists of pins embedded into base materials by means of a gunpowder charge. The effects of fastener type, washer, diameter, length, embedment depth have been investigated and discussed elsewhere (Lamanna et al. 2001; Lamanna 2001). Pre-drilling holes in the concrete is strongly recommended in order to reduce detrimental cracking phenomena. Adequate embedment of the powder actuated fastener is required in order to secure the FRP laminate to the concrete; a minimum embedment of 1 in (25.4 mm) beyond the pre-drilled hole and the use of 45 to 50 mm long fasteners are recommended (Bank and Arora 2007).

The use of the PAF system is particularly suitable when the compression strength of the concrete is less than 4000 psi (27 MPa). The presence of hard aggregates can prevent the fasteners to fully penetrate the concrete substrate (Bank 2004). The PAF installation requires times shorter than for wedge bolts and wedge anchors.

Wedge bolts are single-piece, heavy duty anchors that are driven into pre-drilled holes. Driving of the wedge bolt can be performed with a common rotary drill or impact wrench. As for the PAFs, the efficiency of wedge bolts is dependent on the presence of

hard aggregates. Preliminary studies (Rizzo et al. 2005b) indicate that the use is not recommended for concrete with compression strength greater than 4000 psi (27 MPa), and with hard aggregates in the mix design.

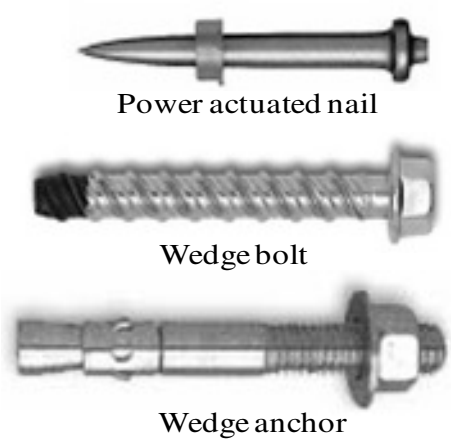

Figure 2.6 – Fasteners used for MF-FRP systems

In spite of longer installation times, wedge anchors can be used for any type of concrete. Concrete wedge anchors are inserted into a hole predrilled into the concrete. The anchors are the driven through the laminate into the hole until the nut and washer are firmly secured against the laminate. The anchors are typically tightened by turning the nut with an electrical drill with torque control, according to the specifications of fastener manufactures.

Fasteners with a 3/8 in (9.525 mm) diameter are recommended for both wedge bolts and wedge anchors. The use of washers is suggested to increase the bearing strength of the connection, similar to the use of resin as a gap filler (Rizzo et al. 2005b).

2.2.3 Behavior of FRP-fastener-concrete connection

The behavior of MF-FRP connections is related to any of the components constituting the connection, which are the concrete substrate, the fastener and the FRP material. As a

result, failure modes can involve the concrete, the yielding/rupture of fastener, or the FRP laminate.

The pryout or spalling of the concrete (Figure 2.7) depends on the local composition of the concrete surface around the fastener. Once pryout failure develops, the fastener rotates and the FRP laminate pulls it out of the concrete. Several factors promote the initiation of the concrete failure, such as a fastener hitting a hard aggregate during installation, low concrete strength, cracked concrete substrate conditions, short edge distance that may cause spalling, and poor fastener embedment depth (Lamanna 2002; Arora 2003).

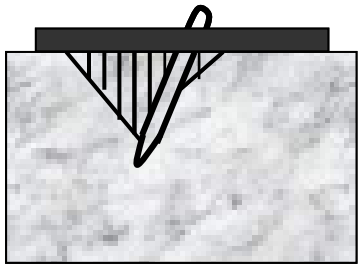

Figure 2.7 – Concrete pryout failure

The fastener failure usually occurs for deep embedment length, low steel strength and large edge distance (Rizzo 2005).

Four typical failure modes can involve the MF-FRP laminate (Figure 2.8): net-tension, cleavage-tension (or block shear), bearing and shear-out (Camanho and Matthew1997; Hassan et al. 1997a; Hassan et al. 1997b). The bearing failure is the most desirable failure mode because the connection is able to maintain its strength until significant levels of displacement (Lamanna 2002; Arora 2003). This failure is characterized by crushing on the material around the bolt-contact area followed by elongation of the hole. The other failure modes tend to develop in a more brittle fashion

(Rosner and Rizkalla 1995). In particular, the net-tension failure is characterized by a fracture in the reduced cross section through the bolt hole, perpendicular to the direction of load. The cleavage failure consists of a crack parallel to the applied load that starts at the edge of the composite and propagates toward the bolt hole, leading to the initiation of other cracks across the net section due to in-plane stress. This failure mode is attributed to a combination of shear and tensile stress in the material. The shear-out failure, considered as a special case of bearing, is characterized by the formation of two cracks parallel to the applied load that propagate from the bolt hole toward the free edge.

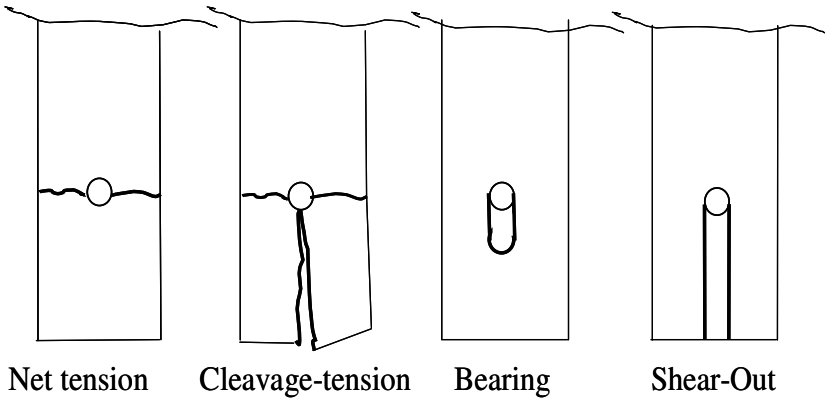

Figure 2.8 – Typical failure modes of mechanically fastened connections in FRP

CHAPTER 3

EXPERIMENTAL PROGRAM

3.1 OVERVIEW

The experimental program consisted of six monotonic tests performed on RC one-way slabs under four-point bending. Four slabs were strengthened with a MF-FRP laminate, a counterpart was strengthened with EB-FRP laminate, while the remaining was used as control specimen.

The specimens were 12 ft (3657.6 mm) long and had a cross section of 12 x 6 in (304.8 x 154.2 mm); the clear span and the shear span were 10 ft (3048 mm) and 4 ft (1219.2 mm), respectively. The flexural reinforcement consisted of three #4 (ϕ=13 mm) bars, resulting in a longitudinal reinforcing ratio of 0.98%; the slabs were designed such that no shear reinforcement was required. A schematic of the loading arrangement is depicted in Figure 3.1.

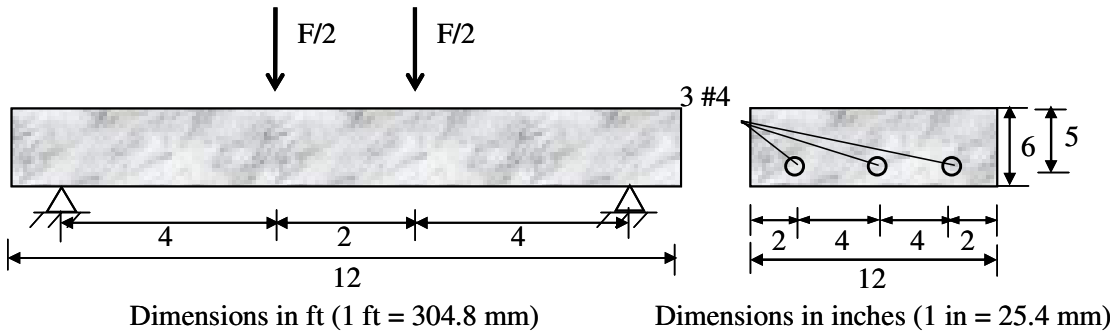

Figure 3.1 – Details of test specimens

3.2 MATERIALS

The slabs were cast from a single batch of Type I portland cement concrete. The concrete strength was determined at test-day by ASTM C39 compression tests on 6 x 12 in (152.4 x 304.8 mm) cylinders; a mean nominal value, f_c, of 3900 psi (26.9 MPa) was found from

all test specimens. Steel Grade 60 was used for flexural reinforcement, as currently adopted for practical applications.

The precured FRP laminates used for the MF-FRP application were manufactured by Strongwell, currently commercialized under the name SAFSTRIP®. The width and thickness are 4 in (101.6 mm) and 0.125 in (3.175 mm), respectively. Powers Wedge Bolts, 1.75 in (44.5 mm) long and 3/8 in (9.525 mm) diameter, were used to attach the FRP laminate to the concrete members. In order to investigate the performance of RC members strengthened with the most practical and simple fastening procedure, no washers nor gap fillers (resin) were used. Figure 3.2 depicts the materials used for strengthening with MF-FRP laminates.

Figure 3.2 – Materials used for strengthening with MF-FRP system

Strengthening with the EB FRP system was performed by using MBRACE CF®130 unidirectional high strength carbon fiber sheets, 0.0065 in/ply (0.165 mm/ply) thick, which were impregnated with MBRACE saturant (an epoxy encapsulating resin). A sheet of 12 in (304.8 mm) width was used; no mechanical anchorages were used for this

application. The mechanical properties of the strengthening materials, as provided by the manufacturers, are listed in Table 3.1.

Table 3.1 – Manufacturer-reported FRP material and fastener properties

Properties	SAFSTRIP® for MF system	MBRACE CF 130* for EB system
Tensile strength	123 ksi (852 MPa)	550 ksi (3800 MPa)
Elongation at rupture %	1.36%	1.67%
Tensile modulus	9020 ksi (62190 MPa)	3300 ksi (227 GPa)
Clamped bearing strength	51. 0 ksi (351 MPa)	-
Unclamped bearing strength	31.0 ksi (214 MPa)	-
Open hole strength	94.6 ksi (652 MPa)	-
Allowable fastener capacity when embedded 1.5 inches (38.1 mm) in 4000 psi (27.4 MPa) concrete: Tension: 665 lb (3.0 kN); Shear: 1220 lb (5.5 kN)**		

*Design values suggested by the manufacturer
**Allowable values are computed with a safety factor of 4

3.3 PRELIMINARY DIMENSIONING AND STRENGTHENING LAYOUTS

The design of the five specimens strengthened with the MF-FRP system and the EB-FRP system was based on an equivalent nominal flexural strength with failure governed by crushing of the concrete after yielding of the steel reinforcement. A nominal strength of the concrete f'_c = 4000 psi (27.6 MPa) and a yielding strength of the steel reinforcement f_y = 60 ksi (413.7 MPa) were assumed in the design.

The design of the member strengthened with the EB system was performed by following the provisions in ACI 440.2R-08 (ACI 2008a); in the analysis of the test specimen, the strength-reduction factor ϕ, the reduction factor Ψ_f for the flexural-strength

contribution of the FRP, and the environmental reduction factor C_E were assumed equal to 1.

The control specimen was designed according to ACI 318-08 (ACI 2008b) provisions, with failure being governed by crushing of the concrete after steel yielding.

Finally, the members strengthened with the MF-FRP system were designed using analytical models available in the technical literature (Arora 2003; Lamanna et al. 2004; Bank and Arora 2007). More details are reported in the following section.

3.3.1 Existing models for members strengthened with MF-FRP system

The existing models are based on strain compatibility, equilibrium and constitutive relations of the materials. For convenience of calculations, they assume no relative slip between the concrete and the FRP laminate when the ultimate capacity is attained. This implies that the strains in the internal steel reinforcement, in the concrete and the FRP can be computed as proportional to the distance from the neutral axis, that is, a plane section before loading remains plane after loading. These models predict with satisfactory approximation the ultimate strength of MF-FRP strengthened beams; however, in such procedures, design optimization and construction guidelines are not addressed. In addition, the actual performance of a member strengthened with a MF-FRP system may differ from the predicted response if some brittle failure modes of the connection are not prevented. Also, if the failure modes of the mechanically fastened connections are all taken into account (Bank and Arora 2007), the complexity of the analysis becomes the main concern. As a result, there is a need of simplifying the analytical procedure that only account for desirable failure modes of the FRP-fastener connection and prevent some brittle behaviors that are undesirable. This can be pursued by selecting proper MF-

FRP reinforcing configurations including fastener types, fastener layouts and minimum edge distances.

3.3.2 Selected MF-FRP configurations

The selected configurations for a typical 4 in (101.6 mm) wide laminate are shown in Figure 3.3. In each configuration, the FRP laminate, 0.125" (3.175 mm) thick, is characterized by two staggered rows of holes. On each row, the holes are spaced 3 in (76.2 mm) on-center. For the lower row, the first hole on the left is at an edge distance of 2.5 in (63.5 mm); while for the upper row, this distance is equal to 4 in (101.6 mm). Each row is at a side distance of 1 in (25.4 mm). The vertical spacing between the rows is equal to 2 in (50.8 mm) on-center. The staggered configuration allows for a better exploitation of the laminate strength, reducing the shear lag occurring when a single row of fasteners is used (Rizzo 2005).

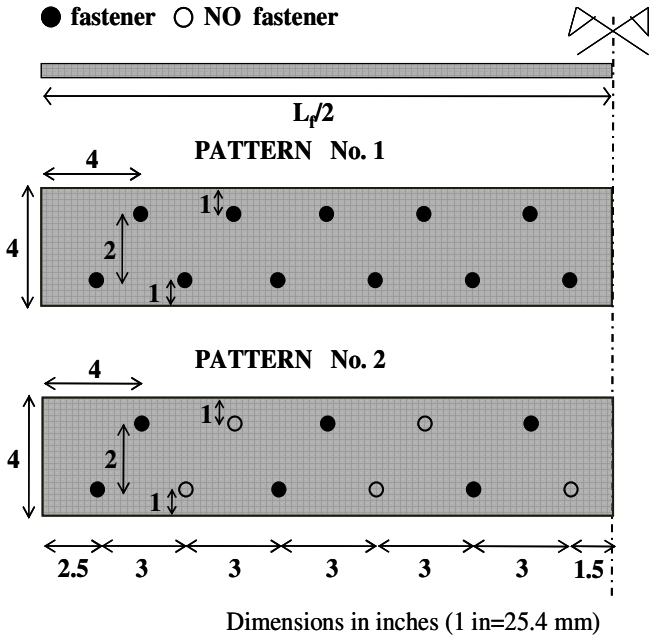

Figure 3.3 – Selected MF FRP fastener layouts

Additionally, the staggered pattern allows for a greater distribution of forces across the width of the strip (Martin and Lamanna 2008). The selected configuration is characterized by two different fastener layouts, identified in Figure 3.3 as follows:

- Pattern No. 1: the number of fasteners is equal to the numbers of pre-dilled holes;
- Pattern No. 2: the fasteners are placed at every second hole.

The selected spacing and fastener layout are suitable for preventing:

- premature shear-out failure between fasteners when bearing occurred;
- concrete substrate failure (pry-out failure);
- cleavage failure.

In order to prevent the occurrence the first two failure modes, 3 in (76.2 mm) fastener on-center spacing is the minimum recommended (Arora 2003; Martin and Lamanna 2008); this is also the minimum value suggested by most fastener manufactures for constructability issues. The brittle pry-out failure, typical when closely spaced fasteners produce high stresses in the concrete substrate, may occur even if the amount of force per fastener is below the limit that causes bearing in the FRP laminate. The overlapping of cone-shaped failure surfaces originated in the concrete substrate when the fasteners are mechanically attached, can cause delamination of the FRP strip. Tests performed by Bank et al. (2002) on large T-beams with closely spaced fasteners have shown this failure mode. In order to prevent the cleavage failure at the end fasteners, the edge distance of 2.5 in (63.5 mm) is the minimum value recommended by Lamanna (2002); additionally, it is also a suitable distance for preventing premature shear-out failures in the FRP strip at the end fasteners (Rizzo 2005). Similar considerations hold for different laminate geometries and properties.

3.3.3. Analytical procedure used for the design of MF-FRP specimens

The analytical procedure adopted herein for the prediction of the nominal flexural strength of RC members strengthened with MF-FRP systems, uses the same assumptions made by existing models (Arora 2003; Lamanna et al. 2004; Bank and Arora 2007). The frame of analysis is similar to that developed to design RC members strengthened with EB-FRP systems adopted per ACI 440.2R-08 (ACI 2008a). The procedure does not account for the improved performance of the connection due to the use of washers and resin. The flexural strength of a section depends on the controlling failure modes and should be ensured by a proper selection of the fastener layouts as depicted in Figure 3.3. Therefore, the following failure modes are investigated for an MF FRP-strengthened section under flexure:

- crushing of the concrete in compression after yielding of the reinforcing steel;
- yielding of the steel in tension followed by bearing failure of the FRP Laminate;
- yielding of the steel in tension followed by net tension failure at open hole of the FRP laminate.

The following assumptions are made:

(1) strains in the steel reinforcement, concrete and FRP are directly proportional to the distance from the neutral axis, that is, a plane section before loading remains plane after loading. This assumption neglects the effect of slip between the steel reinforcing bars and the surrounding concrete and the slip between the FRP strip and the concrete surface. The may be neglected past yielding of the steel. After that, in fact, the laminate can be considered fully engaged, as supported by experimental evidence (Rizzo 2005);

(2) there is uniform stress and strain across the width of the FRP strip. This assumption ignores shear lag and assumes there is no variation in the stress across the width of the strips;

(3) the compressive failure of concrete occurs at a compressive strain of 0.003;

(4) the tensile strength of concrete is neglected,

(5) the steel reinforcement has a perfectly elastic-plastic behavior both in tension;

(6) although the mechanically fastened FRP strip shows some pseudo-plastic behavior after attaining the bearing strength, a linear elastic stress-strain relationship is assumed;

(7) the force from the FRP laminate at any section is distributed uniformly to the fasteners at that section. This assumption implies the force transferred to the FRP strip is directly proportional to the number of fasteners available at the section;

(8) the maximum strain level attainable in the FRP is governed by the lowest associated with three conditions: a) the strain level developed in the FRP when concrete crushes, b) the strain at which bearing failure occurs, and c) the strain at which net tension failure at an open hole in the strip occurs.

The analytical procedure indirectly accounts for concrete substrate failure, cleavage and shear out failure. As previously noted, the prevention of these failures is addressed by the selection of proper fastener spacing and edge distances.

To illustrate the basic concepts of the analytical procedure, Figure 3.4 depicts the internal strain and stress distribution for a singly reinforced rectangular section under flexure at the ultimate stage.

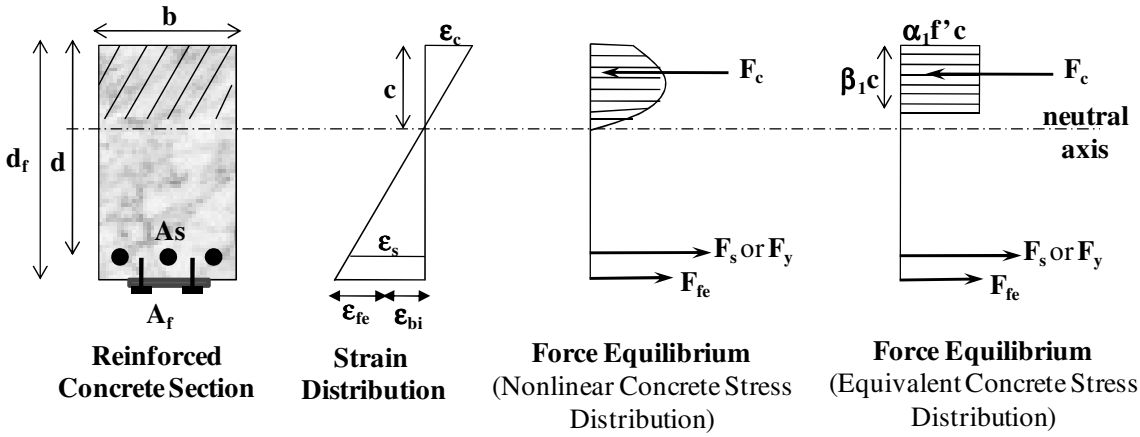

Figure 3.4 – Internal strain and stress distribution at ultimate stage

The procedure involves selecting an assumed depth of the neutral axis, *c*; calculating the strain level in each material; calculating associated stress levels in each material; and checking internal forces equilibrium. If the internal force resultants do not equilibrate, the depth to the neutral axis must be adjusted and the procedure iterated. For any assumed value of c, the strain level in the FRP reinforcement, $\varepsilon_{fe,}$ can be computed by Eq. (3.1) or Eq. (3.2), depending on the controlling failure mode for the assumed neutral axis depth:

$$\varepsilon_{fe} = 0.003 \cdot \frac{d_f - c}{c} - \varepsilon_{bi} \le \varepsilon_{fu} \tag{3.1}$$

$$\varepsilon_c = (\varepsilon_{fe} + \varepsilon_{bi}) \frac{c}{d_f - c} \qquad \varepsilon_{fe} = \varepsilon_{fu} \tag{3.2}$$

where ε_{bi} is the existing state of strain of the member being strengthened; d_f is the effective depth of FRP flexural reinforcement; ε_{fu} is the maximum strain achievable in the FRP reinforcement computed as follows:

$$\varepsilon_{fu} = \min\left(\varepsilon_{fu,b}; \varepsilon_{fu,t}\right) \tag{3.3}$$

where $\varepsilon_{fu,b}$ is the maximum strain at which the bearing failures occurs at an generic section x,, given by Eq. (34); $\varepsilon_{fu,t}$ is the maximum strain at which the strain for net tension failure at open hole in the strip occurs (Eq. [3.5]).

$$\varepsilon_{fu,b} = \frac{T_f}{E_f \cdot A_f} = \frac{\sum_1^n P_f}{E_f \cdot w_f \cdot t_f} = \frac{n \cdot P_f}{E_f \cdot w_f \cdot t_f} \tag{3.4}$$

$$\varepsilon_{fu,t} = \varepsilon^*_{fu} \cdot \frac{A_{net}}{A_f} = \varepsilon_{fu} \cdot \frac{(w_f - \phi) \cdot t_f}{w_f \cdot t_f} \tag{3.5}$$

Eq. (3.4) is based on the assumption that, due to pseudo-plastic behavior of the mechanically fastened connection, the force from the FRP strip at any section, T_f, is distributed uniformly to n fasteners at that section; E_f, w_f and A_f are longitudinal elastic modulus, width and cross section area of the FRP Laminate, respectively; P_f is the maximum bearing load of a single fastener that can be directly evaluated through bolted shear tests for the specific fastener typology used for the connection, or by using Eq. (3.6):

$$P_f = \sigma_b \cdot t_f \cdot d \tag{3.6}$$

where σ_b and t_f are the bearing strength and the thickness of the FRP laminate, respectively, and d is the fastener diameter. In Eq. (3.5), ε_{fu}* is the guaranteed ultimate tensile strain of the FRP laminate estimated by characterization tests, ϕ is the hole diameter.

With the strain and stress level in the FRP and steel reinforcement determined for the assumed neutral axis depth, internal force equilibrium may be checked using Eq. (3.7):

$$c = \frac{(A_s \cdot f_s + A_f \cdot f_{fe})}{\alpha_1 \cdot f'_c \cdot \beta_1 \cdot b} \tag{3.7}$$

where α_1 and β_1 are parameters defining a rectangular stress block in the concrete equivalent to the nonlinear distribution of stress. If concrete crushing is the controlling mode of failure (after steel yielding), α_1 and β_1 can be taken as the values associated with the Whitney stress block, as defined in ACI 318-08 (ACI 2008b).

The calculated and assumed values for c are then compared. If they agree, then the convergence is reached. If the calculated and assumed values do not match, another value for c is selected, and the process is repeated until convergence is attained.

The nominal flexural strength of the section with FRP is then computed:

$$M_n = A_s \cdot f_s \left(d - \frac{\beta_1 \cdot c}{2} \right) + \psi_f A_s \cdot f_{fe} \left(h - \frac{\beta_1 \cdot c}{2} \right) \tag{3.8}$$

where f_s and f_{fe} are the effective level of stress in the steel reinforcement and FRP laminate, respectively. An additional reduction factor, Ψ_f is applied for the flexural-strength contribution of the FRP reinforcement, as recommended by ACI (2008a) for strengthening with EB-FRP systems.

The design flexural strength, ϕM_n, is calculated by multiplying the nominal moment strength M_n, by the strength-reduction factor ϕ. The value of ϕ depends on the strain level in the steel achieved at the ultimate-limit state and can be determined by following the philosophy of ACI 318-08 (2008b). Also, the tensile properties of the FRP laminate should account for the environmental reduction factor C_E (ACI 2008a).

3.3.4 Selection of FRP laminate length

A parametric analysis was performed in order to select the length of the FRP laminate for the considered Pattern No. 1 and Pattern No.2 (Figure 3.3). The results of the

preliminary analysis for Pattern No.1 and Pattern No. 2 are shown in Figures 3.5 and 3.6; for symmetry, only half length of the beams was analyzed.

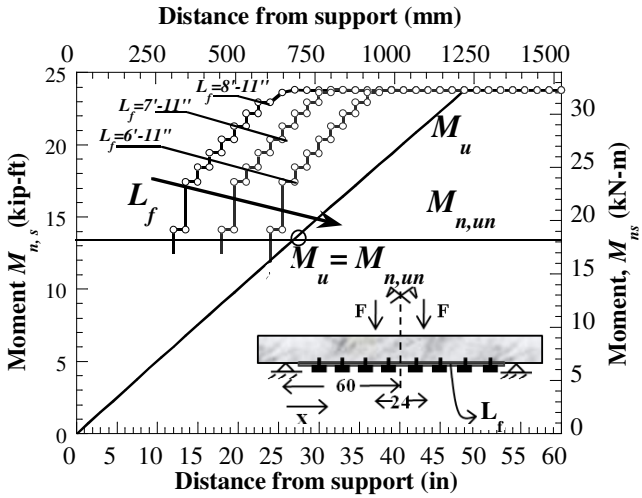

Figure 3.5 – Selection of FRP Laminate length: Pattern No. 1

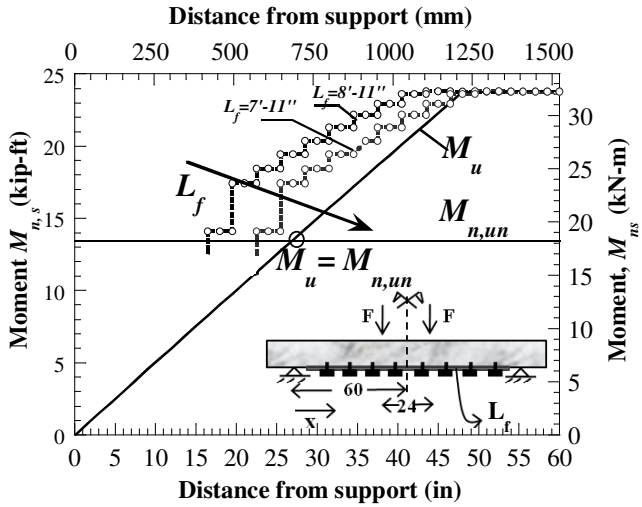

Figure 3.6 – Selection of FRP Laminate length: Pattern No. 2

In each plot, the horizontal solid line $M_{n,un,}$ represents the nominal moment capacity of the unstrengthened slab, which is constant along the length, being constant the internal steel reinforcement in the slab; M_u represents the increased demand which is linear in the shear span and constant in the zero shear region; $M_{n,s}$ identifies the moment capacity of

the MF-FRP strengthened slab for different values of L_f which is the length of the reinforcing FRP laminate. In the constant moment region, $M_{n,s} = M_u$ is set; however, in a realistic case, the demand may be represented by a moment envelope due to a different combination of the loads. For this example, the analytical procedure yields the same moment capacity $M_{n,s}$ in the constant moment region M_u independently on the use of Patter No.1 or Pattern No.2. The moments $M_{n,un}, M_u, M_{n,s}$ refer to the nominal capacity of the member, w, the coefficients C_E and ϕ have been assumed equal to 1. L_f = 8'-11'' (2718 mm), L_f = 7'-11'' (2413 mm), L_f = 6'-11'' (2108 mm) are the length of FRP laminate for which the moment capacity of the member was computed; it was assumed that L_f = 8'-11'' (2718 mm) is the maximum length of the FRP laminate that can be used over a clear span of length L=10 ft (3048 mm).

The parametric analysis consists of calculating the moment capacity at discrete locations along the member by applying the analytical procedure discussed earlier. A length of the FRP laminate has to be first assumed, then, the number of fasteners required for layout is known. At a generic section x, the maximum strain achievable in the FRP can be calculated through Eqs. (3.4) to (3.5); as long as the condition $\varepsilon_{fu,t} < \varepsilon_{fu,b}$ is verified, and the failure is governed by the crushing of the concrete after the steel has yielded, the moment capacity M_{ns} remains constant; this means that additional fasteners do not contribute to increasing the capacity of the member. In the particular cases of Figures 3.5 and 3.6, the computation of the moment capacity has been performed by increasing the distance x from the supports by an increment of 1.5 in (38.1 mm); this increment corresponds to the spacing between staggered fasteners in Pattern No.1. The

procedure can be repeated for decreasing values of L_f until the intersection of the capacity and demand curves is reached.

The $M_{n,s}$ curves are arrested for value of moments less than $M_{n,s}$ where the optimization procedure loses significance, being in these conditions, $\varepsilon_{fu} = \varepsilon_{fu,b}$ with $\varepsilon_{fu,b}$ resulting by the contribution of a limited number of fastener. However, in the region for which the procedure yields $M_{n,s} < M_{n,u}$ the length of the FRP reinforcement has to be still accounted for the determination of the development length of the laminate. In the case examined, the development length is equal to 19.5 in (495.3 mm). The results of the parametric analysis show that L_f = 6'-11'' (2108 mm) is the selected length for the FRP Laminate if Pattern No.1 is used; L_f = 7'-11'' (2413 mm) is the chosen value if Pattern No.2 is considered.

Table 3.2 reports the main data of the strengthening systems used for test specimens. Such data include: number of laminates; width (b_f), thickness (t_f) and length (L_f) of the laminate; fastener layout (Pattern No.1 or No.2) and total number of fasteners in the clear span. Labels C and EB refer to the control specimen and member strengthened with externally bonded carbon FRP laminate, respectively.

According to the results of parametric analysis, specimens MF-1-L and MF-1-S were both MF-FRP strengthened using the same fastener layout (Pattern No.1) but with a different length of FRP laminate ("L" stands for longer laminate; "S" for shorter laminate): in particular, the former was strengthened with one FRP laminate having length L_f = 8'-11" (2718 mm); the latter, with a shorter length L_f = 6'-11" (2108 mm). Similarly, specimens MF-2-L and MF-2-S were both strengthened by using Pattern No.2

but with one FRP laminate having length L_f = 8'-11" (2718 mm) and L_f =7'-11" (2413 mm), respectively.

Table 3.2 – Main data of the strengthening systems used for tests specimens

Slab	# of laminates	b_f in (mm)	t_f in (mm)	L_f in (mm)	Pattern. No.	# of Fasteners
C	-	-	-	-	-	-
EB	1	12 (304.8)	0.0065* (0.165)	113 (2865)	-	-
MF-1-L	1	4 (101.6)	0.125 (3.175)	107 (2718)	1	67
MF-1-S	1	4 (101.6)	0.125 (3.175)	83 (2108)	1	51
MF-2-L	1	4 (101.6)	0.125 (3.175)	107 (2718)	2	35
MF-2-S	1	4 (101.6)	0.125 (3.175)	95 (2413)	2	29

*Nominal fabric thickness

3.4 STRENGTHENING PROCEDURE

The slabs were placed upside down prior to the application of the FRP laminate. For the strengthening with MF-FRP system, the composite laminates were cut to the required length and the fastener locations were marked. Each laminate was predilled with a rotary drill and then was centered on the concrete member from side to side and end to end and held in place at each end. For specimens MF-1-L and MF-2-L, the strip was terminated 6.5 in (165.1 mm) from the supports; for MF-1-S and MF-2-S, 18.5 in (470 mm) and 12.5 in (31.75 mm), respectively. Installation of bolts was also preceded by predrilling using the provided Powers Wedge Bit, mounted on a rotary hammer drill. Holes were drilled into the base material to an approximate depth of 0.25 in (6.35 mm) deeper than the

required embedment length, equal to1.5 in (38.1 mm), as recommended by the manufacturer; a maximum clamping torque of 40 lb-ft (54.2 N-m) was applied to tight the fasteners. The strengthening procedure, including predrilling of the laminate, predilling of holes into the concrete, cleaning of the holes, placing and tightening of the bolts, took approximately 40 minutes for each specimen. Figure 3.7 shows salient steps of the strengthening procedure with MF-FRP system and the final configuration for the specimen MF-1-L.

Figure 3.7 – Strengthening procedure of specimen MF-1-L

The slabs were then returned to an upright position with the tensile steel on the bottom and placed on the supports.

For the EB-FRP system, before the impregnating resin was applied, the surface of the member was primed, and then the putty was applied onto the substrate. The epoxy adhesive was allowed to cure for a minimum of 24 hours as recommended by the manufacturer. The strengthening procedure, took approximately 2 hours (Figure 3.8).

Figure 3.8 – Strengthening procedure of specimen EB

3.4 TEST SETUP AND INSTRUMENTATION

Specimens were tested in four-point bending over a 10 ft (3048 mm) clear span with a constant moment region of 2 ft (610 mm). Tests were conducted in load control; a hydraulic jack was used to apply the load and a steel spreader beam distributed it on the two loading sections (Figure 3.9). Load-unload cycles were imparted at different stages during the tests. the loading was halted periodically to allow marking the cracks.

In all tests, LVDTs were used to measure the deflection at midspan and the settlement at the supports. Strain gauges were arranged to measure the compression strain in concrete and the tensile strain in the steel reinforcement at midspan. For the specimens strengthened with MF-FRP system and EB-FRP system, strain gauges were also used to measure the strain in the FRP laminate at different locations, usually spaced 12 in (304.8 mm) apart. The schematic of Figure 3.10 shows the typical instrumentation used for the FRP strengthened specimen.

Figure 3.9 – Test setup

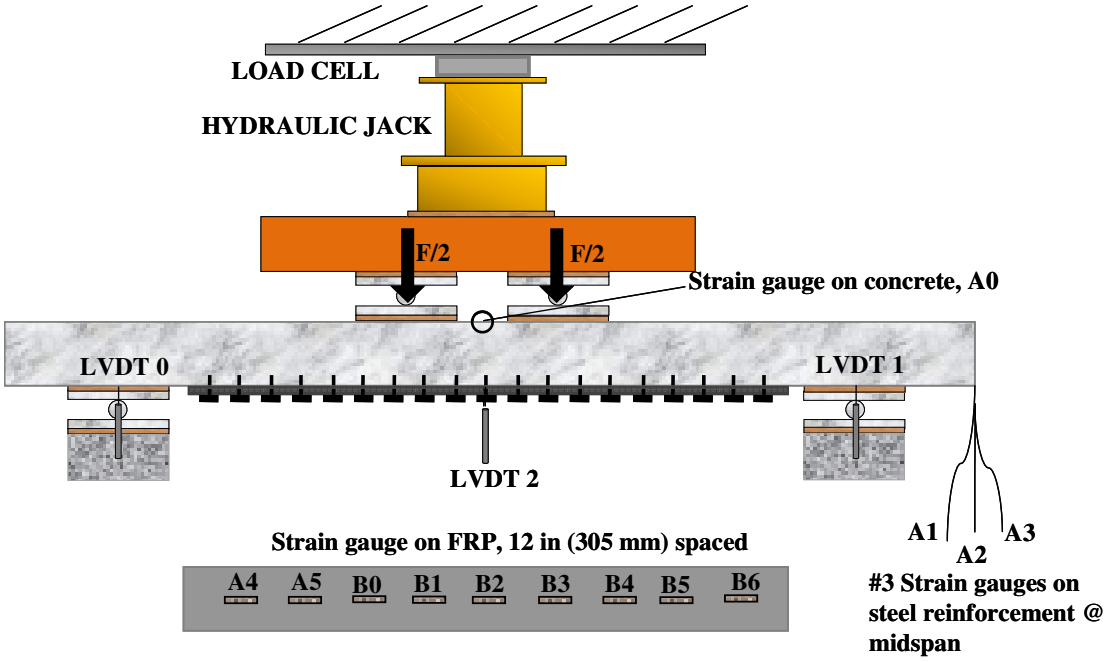

Figure 3.10 – Typical instrumentation of FRP strengthened test specimens

CHAPTER 4

DISCUSSION OF TEST RESULTS

4.1 OVERVIEW

This chapter presents the experimental results for all of the six specimens. As it will be noted, the critical issue raised by the analysis of data for specimens strengthened with the MF-FRP system is the significant slip occurring between FRP and concrete substrate. This phenomenon may significantly affect the validity of some assumptions made in the design procedure adopted. As a result, further studies will be required to quantify the slip occurring between FRP and concrete and improve the efficiency of existing analytical models at loads other than ultimate.

4.2 FAILURE MODES

The failure modes in all test specimens are depicted in Figures 4.1 through 4.4. Figure 4.1 shows the crack pattern experienced in the control specimen. The first flexural crack initiated at midspan under a load of about 2 kip (8.9 kN); then, further flexural cracks developed along the constant moment region along with flexural-shear cracks towards the supports. Significant deflection was exhibited at the maximum load. Failure of the member was characterized by crushing of the concrete at midspan after yielding of steel bars.

For the EB-FRP specimen, although crushing of the concrete after steel yielding was the expected failure mode, a premature intermediate debonding of the CFRP laminate was experienced (Figure 4.2). Debonding initiated at a section near the region of maximum moment. At increasing loads, the cracks opened and induced high interfacial shear stress causing FRP debonding, which propagated outwards along the shear span.

This failure did not result in the concrete cover to separate from the rest of the RC member.

Figure 4.1 – Crack pattern and failure: control specimen

Figure 4.2 – Debonding failure exhibited by the specimen EB

The ultimate failure mode in the members strengthened with the MF-FRP system was characterized by crushing of the concrete after yielding of the steel. However, for specimens MF-1-S and MF-2-L, as the steel reinforcement approached yielding, flexural cracks outside of the constant moment region turned into inclined flexural-shear cracks.

At failure, the high concentration of shear force caused spalling of the concrete cover. A similar behavior was experienced in some tests performed by Lamanna (2002).

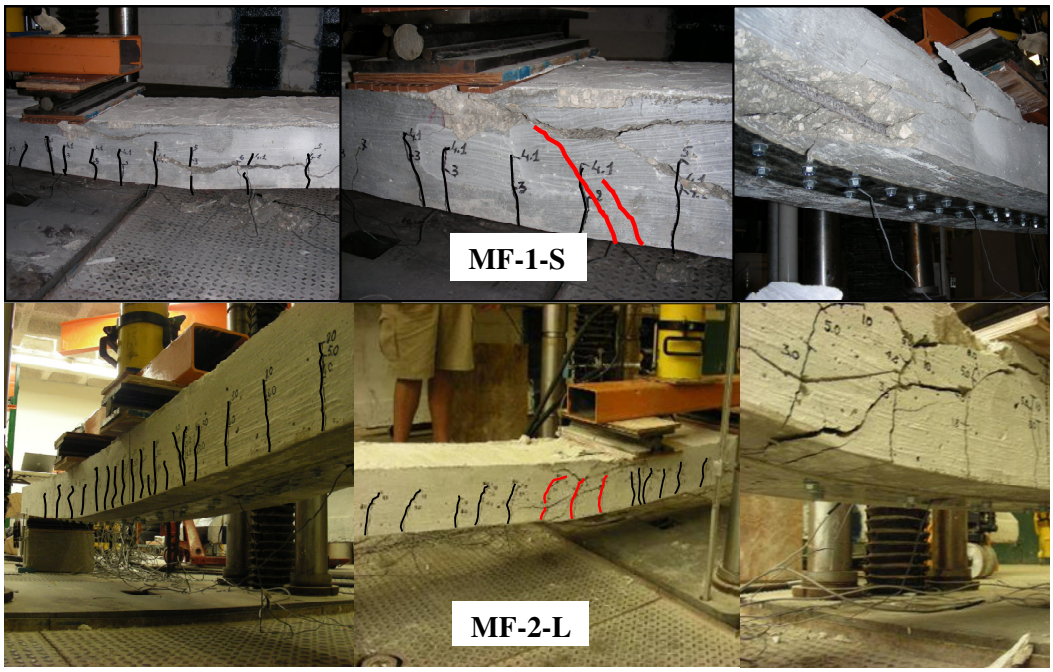

Figure 4.3 – Crack pattern and failure modes in the slabs MF-1-S and MF-2-L

For both specimens, concrete crushing was experienced near one of the loading sections. Figure 4.4 shows the crack pattern and failure mode in the remaining specimens: compression failure of the concrete was experienced in both specimens; crushing was attained at the midspan, for specimen MF-1-L, and near one of loading sections for specimen MF-2-S.

For all members strengthened with the MF-FRP system, the first flexural cracks developed at about 2 kips (8.9 kN). A significant distribution of cracks was observed along the members early after the cracking moment was attained. This phenomenon was

caused by the local damage of the concrete induced by predrilling. No detachment of the FRP laminate from the concrete surface was observed at failure.

Figure 4.4 – Crushing of the concrete in the slabs MF-1-L and MF-2-S

Finally, the scenario of failure modes observed for the MF-FRP specimens evidenced that the selection of fastener layout was appropriate for preventing detrimental brittle failures of the connection. No premature shear-out failure, cleavage, and pry-out failure was experienced.

4.3 STRENGTH AND DEFORMABILITY

Table 4.1 summarizes the failure modes of the members and reports the main results of tests in terms of moment and displacement; the concrete compressive strength, f_c, determined at test-day by compression tests on 6 in x 12 in (152.4 x 304.8 mm) cylinders per ASTM C39, is also listed for all of the specimens. The yield moment M_y (and the corresponding deflection δ_y) was defined as the level at which the load deflection curve deviated from linearity; the ultimate moment M_u (and the corresponding deflection δ_u) was defined as the level at which the maximum load was reached. From

Table 4.1 – Summary of slab test results

Slab	f_c psi	M_y k-ft	I_{My} %	M_u k-ft	I_{Mu} %	δ_y in	$I_{\delta y}$ %	δ_u in	$I_{\delta u}$ %	Failure mode
C	3926	13.0	-	17.4	-	1.00	-	3.61	-	YS-CC
EB	3936	15.4	18.5	25.4	46.5	0.89	-11.0	2.34	-35.2	ID
MF-1-L	4134	15.2	16.9	27.5	58.6	0.92	-11.0	2.69	-25.5	YS-CC
MF-1-S	4134	16.0	23.1	25.3	45.5	1.00	-	2.33	-35.5	YS-FS-CC
MF-2-L	3663	15.6	20.0	25.0	44.1	1.00	-	2.86	-20.8	YS-FS-CC
MF-2-L	3663	15.0	15.4	22.7	30.9	1.10	10.0	2.62	-27.4	YS-CC

(U.S. Units)

Slab	f_c MPa	M_y kN m	I_{My} %	M_u kN m	I_{Mu} %	δ_y mm	$I_{\delta y}$ %	δ_u mm	$I_{\delta u}$ %	Failure mode
C	27.1	17.6	-	23.5	-	25.4	-	91.4	-	YS-CC
EB	27.1	20.9	18.5	34.5	46.5	22.9	-11.0	58.4	-35.2	ID
MF-1-L	28.5	20.6	16.9	37.3	58.6	22.9	-11.0	68.6	-25.5	YS-CC
MF-1-S	28.5	21.7	23.1	34.3	45.5	25.4	-	58.4	-35.5	YS-FS-CC
MF-2-L	25.5	21.2	20.0	33.9	44.1	25.1	-	73.7	-20.8	YS-FS-CC
MF-2-L	25.5	20.3	15.4	30.8	30.9	25.4	10.0	66.0	-27.4	YS-CC

(S.I. Units)

YS-CC = concrete crushing after steel yielding; ID = intermediate debonding; YS-FS-CC = after steel yielding, concrete crushing was preceded by the propagation of extensive flexural shear cracks.

$$\%\, I_{M_{y/u}} = \frac{strengthened - unstrengthened}{unstrengthened}; \quad \%\, I_{\delta_{y/u}} = \frac{strengthened - unstrengthened}{unstrengthened}$$

Table 4.1 it can be observed that the slabs strengthened with MF-FRP systems exhibited increases in yield moment over the control specimen ranging from 15.4 to 23.1%, and increases in ultimate moment ranging from 30.9 to 58.6%. In addition, test results show that the MF-FRP system results in a strength increase comparable to that attained with the EB-FRP system. The maximum moment, M_u = 27.5 kip (37. 3 kN m) was achieved by the specimen MF-1-L, strengthened using Pattern No.1 and L_f = 107 in (2717.8 mm). Figure 4.5 shows the moment-deflection curves for all test specimens.

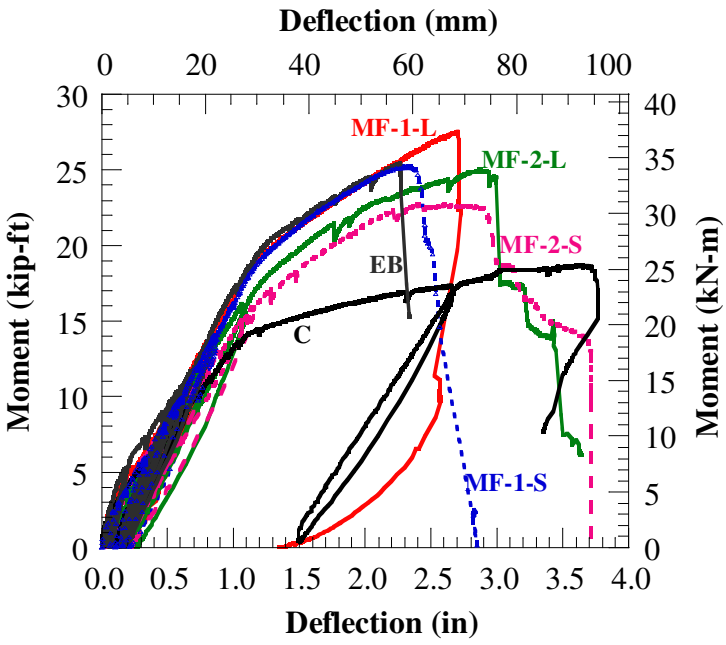

Figure 4.5 – Comparison of moment-deflection curves

The comparison among the experimental curves of the MF-FRP strengthened members evidences that: 1) spacing of fasteners and length of the FRP laminate play a critical role in the performance of the system; 2) an appropriate combination of these two parameters allows for increasing the deformability of the system without significantly affecting the performance in terms of strength. In fact, unlike the strengthening with EB-FRP system, where a significant deformability decrease of the member is always obtained, in the MF-FRP systems design optimization may improve the overall performance of the system. This performance is a function of laminate utilization, or the ability of a fastener pattern to transfer stress from the tensile concrete to the strip. A large number of fasteners means that the stresses are divided in smaller increments; a laminate will never reach its full capacity, which would allow the strip to behave in a "pseudo-ductile" mode, thus the laminate is underutilized. A small number of fasteners divides the forces into larger quantities, which will in turn be transferred to the strip, bringing bearing stresses in the

strip at the fastener closer to the laminate limit, fully utilizing the laminate. From these considerations, it results that the use of 3 in (152.4 mm) staggered Pattern No.2 with a reduced length of the laminate, is the optimal choice. However, it is important to consider the effect of strengthening loss, or system redundancy when evaluating the behavior for field use. In this case, it should be not noted that a greater number of fasteners in the shear span would enable to better account for the loss of a fastener capacity due to vandalism, concrete substrate deficiencies, or potential screw loosening under repeated loading.

The preyield behavior of all strengthened slabs does not show relevant differences, and a small increase of stiffness over the control beam was observed. In the post-yielding stage, the behavior changes as the FRP laminate is providing a significant tensile contribution. In case of members MF-1-L and MF-2-S, where 1.5 in (152.4 mm) staggered Pattern No.1 was used, as stated earlier, the large number of fasteners prevented the strip from reaching its full capacity, which would have allowed the system to behave in a "pseudo-ductile" mode. As a result, these members showed analogous behavior to the EB specimen; under the same moment, no deformability increase over the EB members was measured. Conversely, in the case of specimens MF-2-L and MF-2-S, the post-yielding behavior played a critical role and a better utilization of the laminate was attained. Also, a correlation between the number of fastener and the post-yield deformability of the strengthening system can be observed. The smaller the number of fasteners used in the system, the greater the ductility and the lower the stiffness; conversely, the systems were stiffer when larger number of fasteners were used, but failed at a much smaller displacement. This can be explained by observing the damage

level of the FRP laminate for the specimens MF-1-S and MF-2-S, as seen in Figure 4.6: increasing the spacing implies increasing the load on each fastener, resulting in a greater level of bearing per fastener and better utilization of the laminate. Similar considerations were found by other authors (Martin and Lamanna 2008).

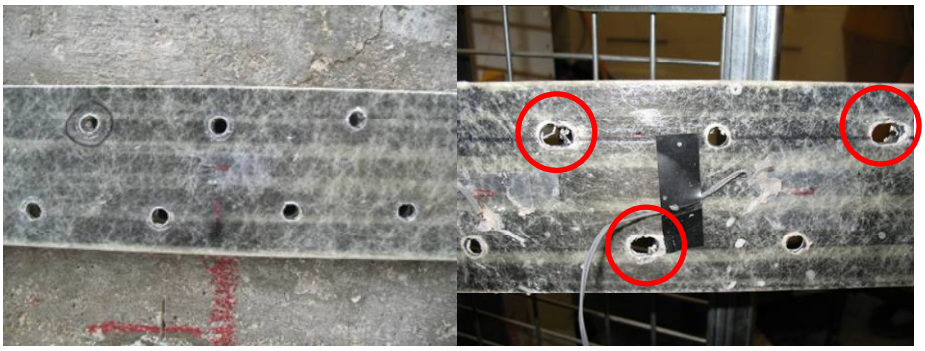

Figure 4.6 – Level of damage of the FRP strip for slabs MF-1-S and MF-2-S

From the comparison between the specimen MF-1-S and MF-2-L for the same moment capacity, the deformability increases from 2.3 in (58.4 mm) for MF-1-S, to 2.9 in (73.7 mm) for MF-2-L. Further details on displacement results are listed in Table 4-1. For the control specimen, the large failure displacement and the significant increase in the post-yield strength is attributed to the low reinforcement ratio and the strain hardening of the steel reinforcement.

4.4 STRAIN DISTRIBUTION

Table 4.2 reports the strain data recorded for steel reinforcement (ε_s^{mid}), concrete (ε_c^{mid}) and FRP (ε_f^{mid}) at the midspan of the test specimens. Also, the value of the maximum strain ε_f^{max} in the FRP is provided when it was attained at different location

from the midspan. It is worth noting that, since crushing of the concrete typically occurred at either loading section, the concrete strain recorded at the midspan was generally smaller than expected values at failure.

Table 4.2 – Slabs strain data

Slab	ε_s^{mid} (με)	ε_c^{mid} (με)	ε_f^{mid} (με)	ε_f^{max} (με)
C	18371	3970	-	-
EB	12300	2050	7697	8090
MF-1-L	10865	3310	6500	-
MF-1-S	7125	2505	2894	4093
MF-2-L	10332	2181	4055	4840
MF-2-S	8624	1674	4626	-

Slab C. Figure 4.7 shows the strain distribution in the concrete and steel reinforcement for the control specimen. The failure mode consisting of crushing of the concrete preceded by yielding of the steel is clearly observed.

Slab EB. Figure 4.8 shows the strain distribution in the FRP laminate for the EB-FRP specimens. Strain gauges were placed at midspan, at the two loading sections and at regular intervals along the laminate in order to evaluate the FRP strain profile. No significant strain levels were recorded near the ends of the FRP laminate. In the constant moment region, after steel yielding, the strain in the FRP rapidly increased until debonding failure occurred.

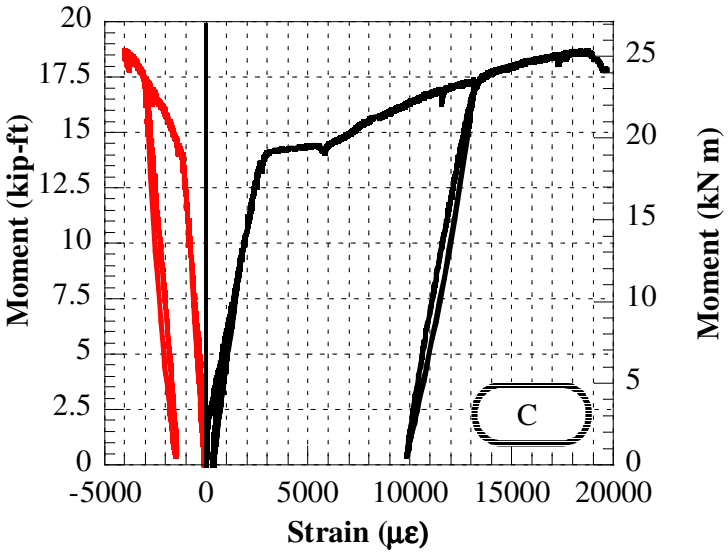

Figure 4.7 – Strain in concrete and steel: slab C

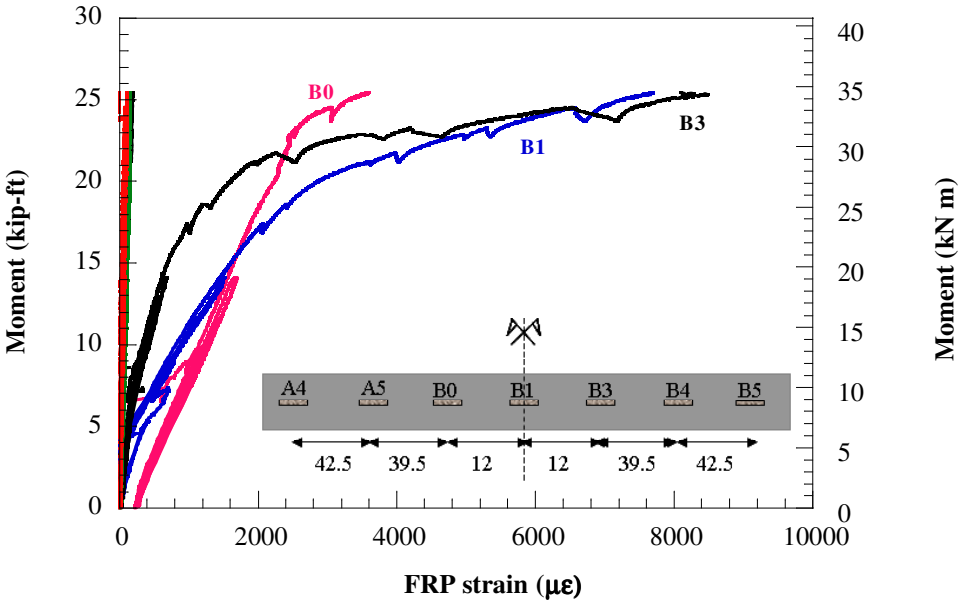

Figure 4.8 – Strain in FRP laminate: slab EB

Figure 4.9 depicts the FRP strain profile for increasing values of the applied moment. A nonlinear strain distribution is observed since the early stages of loading. Also, the

significant increase of strain at the location of strain gauge B3, where the debonding initiated, can be noted starting from moment of 22 kip-ft (29.8 kN m).

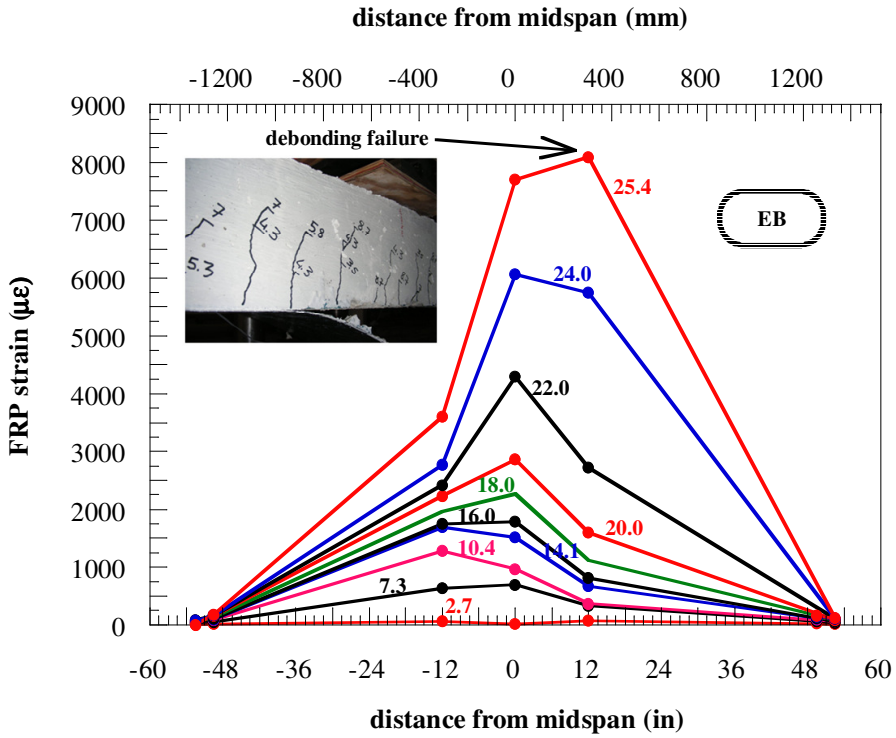

Figure 4.9 – FRP strain profile: slab EB (Moment in kip-ft: 1 kip-ft=1.356 kN m)

Slab MF-1-L. Figure 4.10 shows the strain distribution in the FRP laminate for specimen MF-1-L. Strain gauges were placed along the FRP laminate at a spacing of 12 in (304.8 mm). The readings show that there is a significant increase in the FRP strain after the steel yielding; at that time, the laminate may be considered fully engaged. However, as it will be shown later, slip phenomenon prevalently due to cracks propagation causing partial fastener rotation and bearing mechanism was also exhibited at that stage. The maximum strain was recorded at midspan, achieving a value of 6500 με. Figure 4.11 depicts the FRP strain profile for increasing values of the moment. A

fairly linear and symmetric strain distribution is observed at increasing loads. This shows that the load is transferred evenly among the fasteners in the shear span.

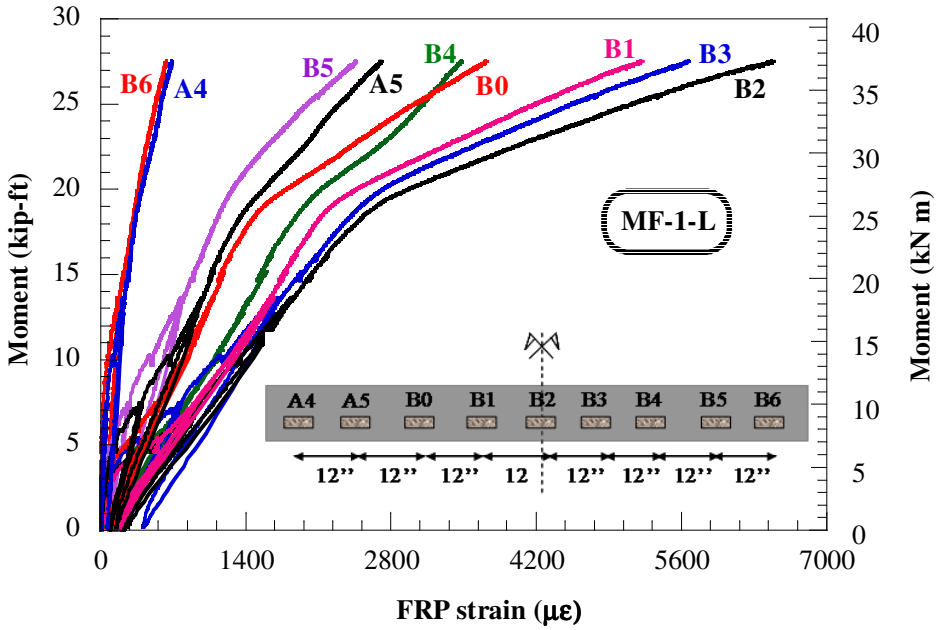

Figure 4.10 – Strain in FRP laminate: slab MF-1-L

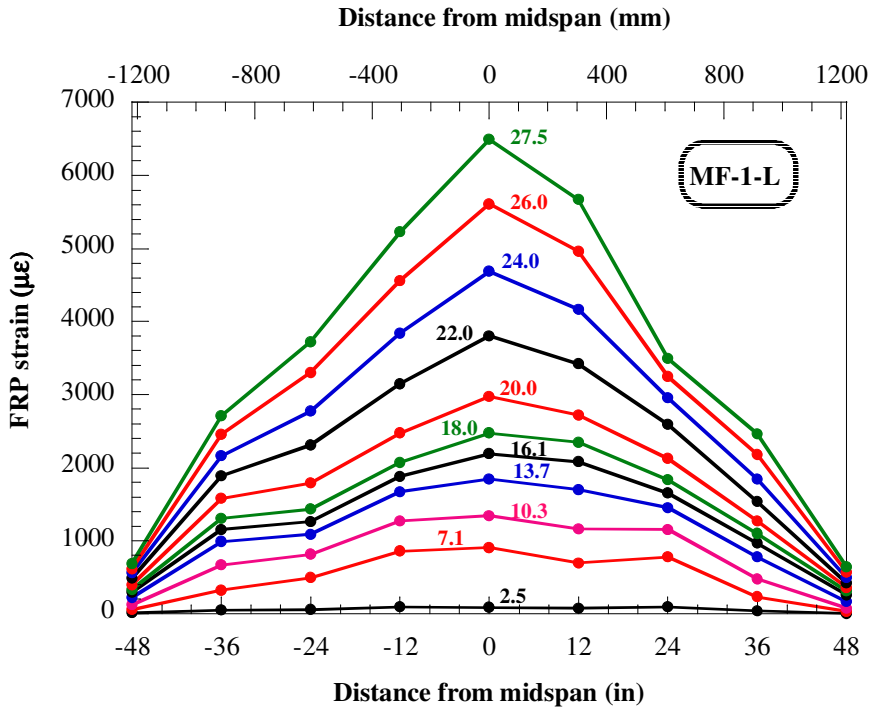

Figure 4.11 – FRP strain profile: slab MF-1-L

(Moment in kip-ft: 1 kip-ft=1.356 kN m)

Slab MF-1-S. Figure 4.12 shows the strain distribution in the FRP laminate for specimen MF-1-S. Strain gauges were placed along the FRP laminate at a spacing of 12 in (304.8 mm). At smaller values of loads, the readings show a limited contribution of the FRP to the total moment due to the slip occurring between the FRP and the concrete substrate. At this stage the slip mechanism is prevalently due to presence of gaps in the connection components and cracks opening causing partial rotation of the fasteners. The FRP contribution increases when the laminate is fully engaged, but at failure low values of the strain are recorded because of slip components. The maximum strain, equal to 4093 με, was achieved at one of the loading points. Figure 4.13 depicts the FRP strain profile for increasing values of the moment. The nonlinear strain distribution may have been affected by the propagation of significant flexural-shear cracks.

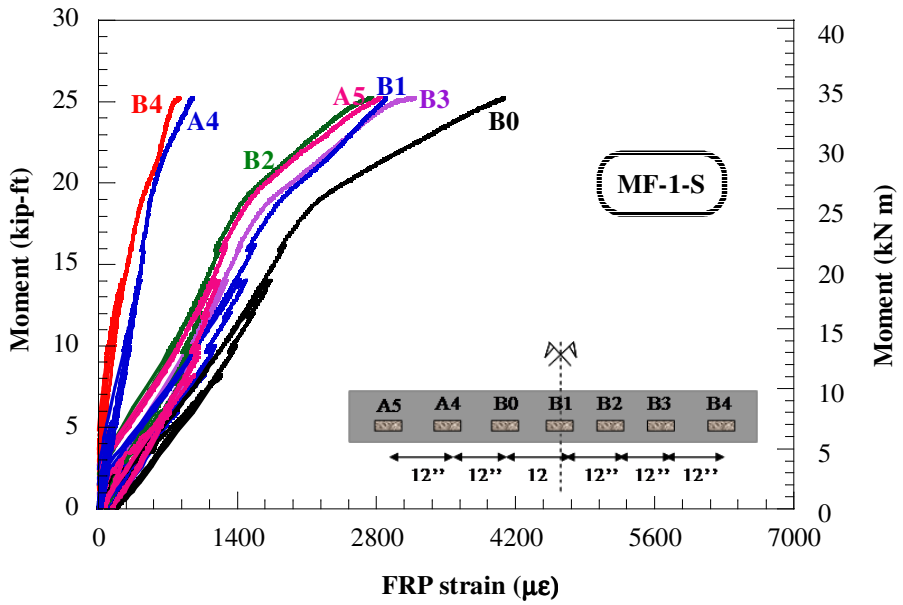

Figure 4.12 – Strain in FRP laminate: slab MF-1-S

Slab MF-2-L. Figure 4.14 shows the strain distribution in the FRP laminate for specimen MF-2-L. Strain gauges were placed along the FRP laminate at a spacing of 12

in (304.8 mm). Also for this test, the readings show that there a significant strain increase after steel yielding.

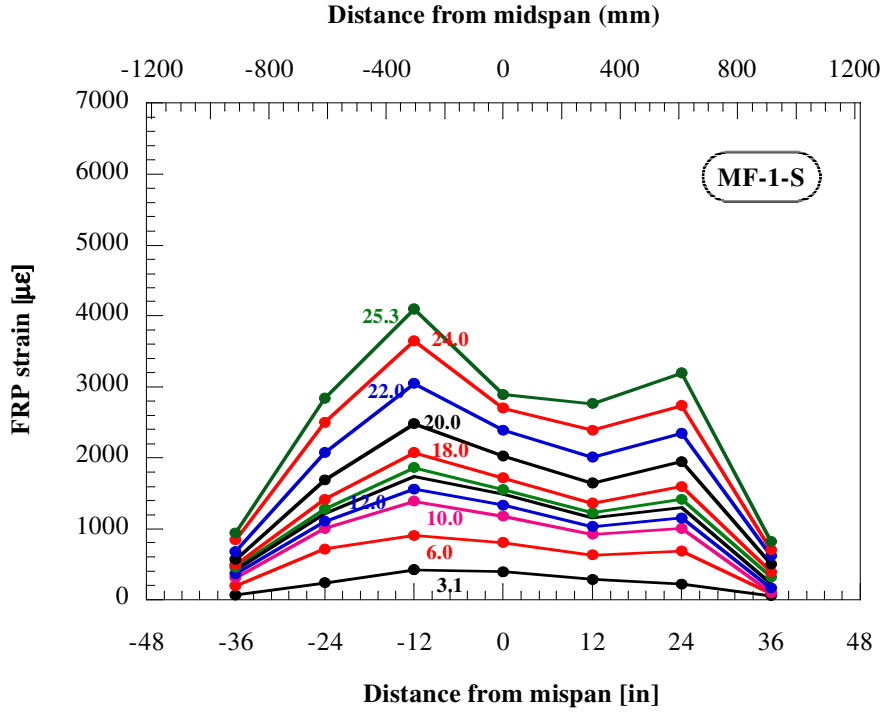

Figure 4.13 – FRP strain profile: slab MF-1-S

(Moment in kip-ft: 1 kip-ft=1.356 kN m)

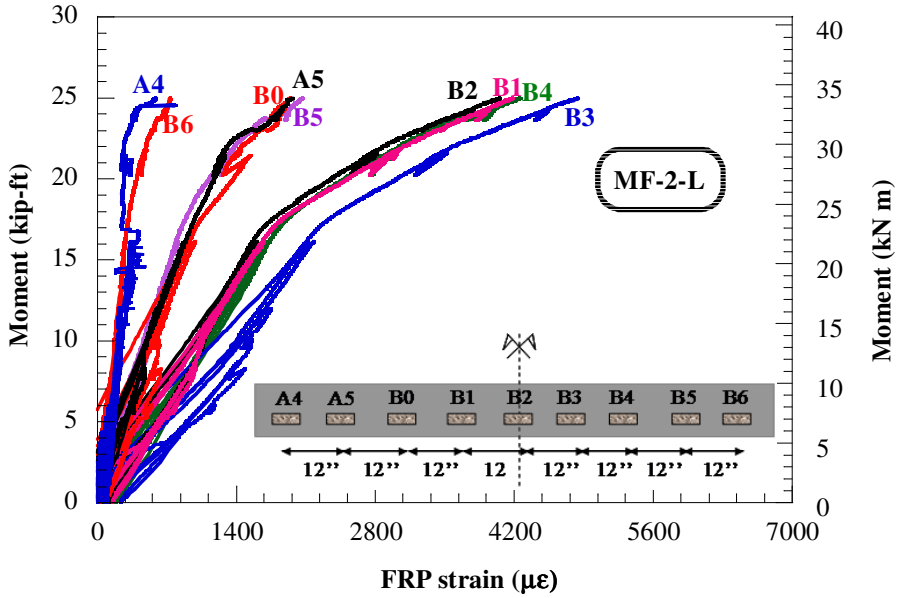

Figure 4.14 – Strain in FRP laminate: slab MF-2-L

The maximum strain, equal to 4840 με, was achieved at one of the loading sections. Figure 4.15 depicts the FRP strain profile for increasing values of the moment. As for the case of specimen MF-2-L, the nonlinear strain distribution may be affected by the propagation of significant flexural-shear cracks. The maximum strain was achieved at the symmetric location to that where failure occurred.

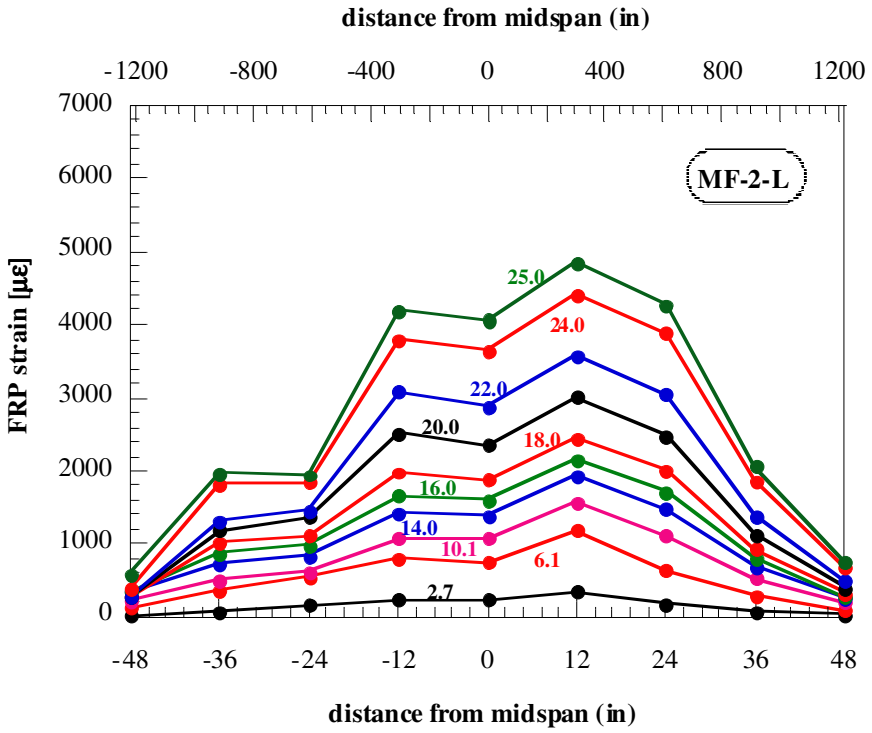

Figure 4.15 – FRP strain profile: slab MF-2-L

(Moment in kip-ft: 1 kip-ft=1.356 kN m)

Slab MF-2-S. Figure 4.16 shows the strain distribution in the FRP laminate for specimen MF-2-S. Strain gauges were placed along the FRP laminate at a spacing of 12 in (304.8 mm) and 6 in (152.4 mm) near the termination of the laminate. The maximum strain, equal to 4626 με, was achieved at midspan.

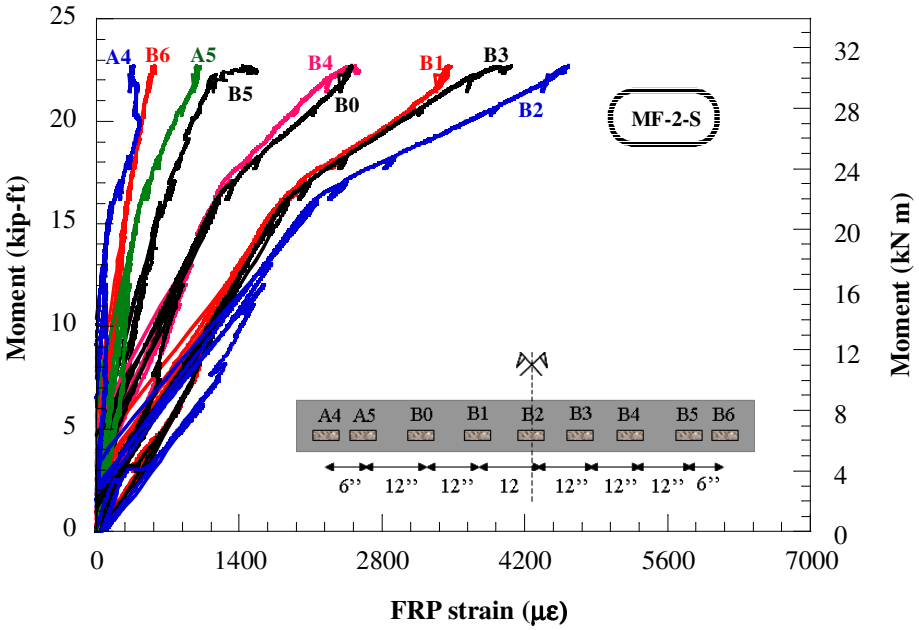

Figure 4.16 – Strain in FRP laminate: slab MF-2-S

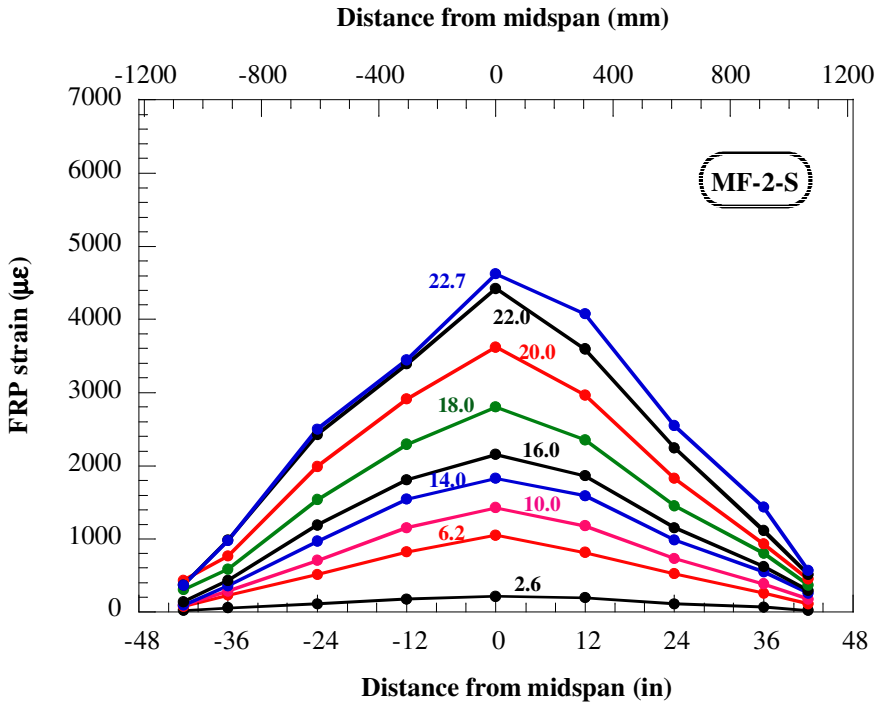

Figure 4.17 – FRP strain profile: slab MF-2-S

(Moment in kip-ft: 1 kip-ft=1.356 kN m)

Figure 4.17 depicts the FRP strain profile for increasing values of the moment. As for specimen MF-1-L, the strain distribution is linear throughout the loading history

4.5 WEAKNESS OF THE EXISTING STRENGTH MODELS

In Table 4.3, comparisons between experimental results and analytical estimates are listed. Also, the estimated values of strains in the concrete (ε_c), steel (ε_s) and FRP (ε_f) are reported to be compared with the experimental ones listed in Table 4.2. *M_n is the estimated value calculated considering ϕ=1 and Ψ_f=1, respectively. The comparison shows a good agreement between experimental and analytical results for the members strengthened with the MF-FRP system. However, the comparison in terms of strains may show significant weaknesses of the existing strength models. As evidenced in Chapter 3, these models are based on the plane section assumption, that is, no slip between the FRP laminate and concrete is assumed.

Table 4.3 – Experimental results and analytical predictions

;

Slab	M_u^{exp} k-ft (kN m)	*M_n k-ft (kN m)	*diff. %	ε_c με	ε_s με	ε_f με
C	17.4 (23.5)	-	-	0.003	12000	-
EB	25.4 (34.5)	22.3 (30.2)	-12.2	0.003	6460	8356
MF-1-L	27.5 (37.3)	25.8 (34.8)	-6.7	0.003	5150	6779
MF-1-S	25.3 (34.3)	25.8 (34.8)	-2.0	0.003	5150	6779
MF-2-L	25.0 (33.9)	25.8 (34.8)	-3.2	0.003	5150	6779
MF-2-S	22.7 (30.8)	25.8 (34.8)	+13.6	0.003	5150	6779

$$\%\ diff = \frac{M_n - M_u^{exp}}{M_u^{exp}}$$; *ϕ=1 and Ψ_f=1

Figures 4.18 and 4.19 depict the variation, in case of test MF-1-L taken as a representative, of the depth to the neutral axis calculated by means of the experimental

values of the strain in the concrete, steel and reinforcement. In Figure 4.18, the neutral axis was calculated considering the linear strain distribution between the concrete and the FRP. In Figure 4.19, the neutral axis was calculated considering the linear strain distribution between the concrete and the steel reinforcement, as typically assumed for RC sections. The comparison between Figure 4.18 and 4.19 clearly shows that the conservation of plane section assumption cannot be accepted. Issues related to the estimation of the actual depth to the neutral axis and of the effective level of strain in the FRP laminate are visibly shown.

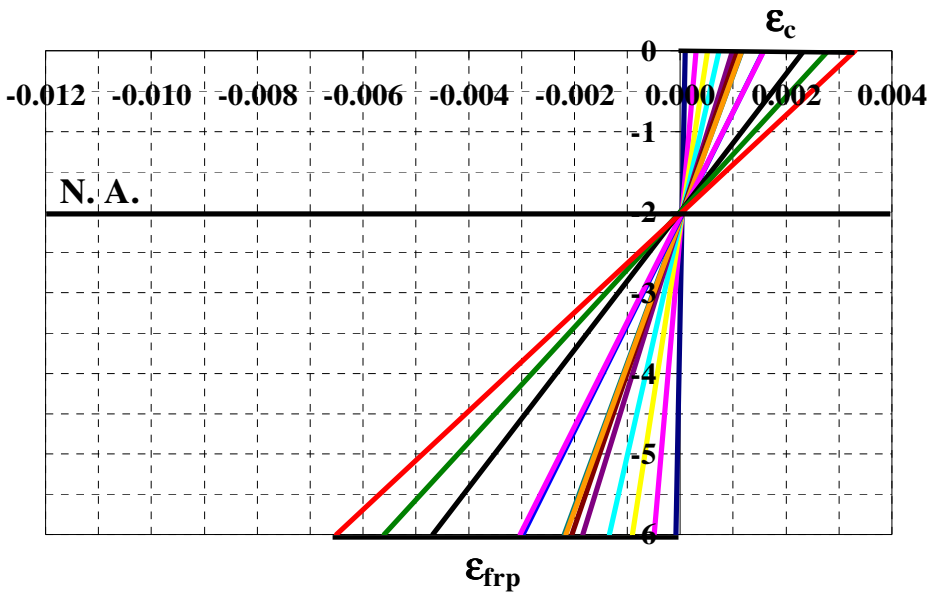

Figure 4.18 – Variation of the depth to the neutral axis with increasing applied moment: linear strain distribution between the concrete and the FRP

Figure 4.20, depicts the effective variation, in case of test MF-1-L, of the depth to the neutral axis for some values of the applied moment: before yielding, at yielding, and after yielding. The concrete in compression is assumed to follow the stress-strain model developed by Park and Paulay (1975), as shown in Figure 4.21; the steel in tension is assumed to have a perfectly elastic-plastic behavior.

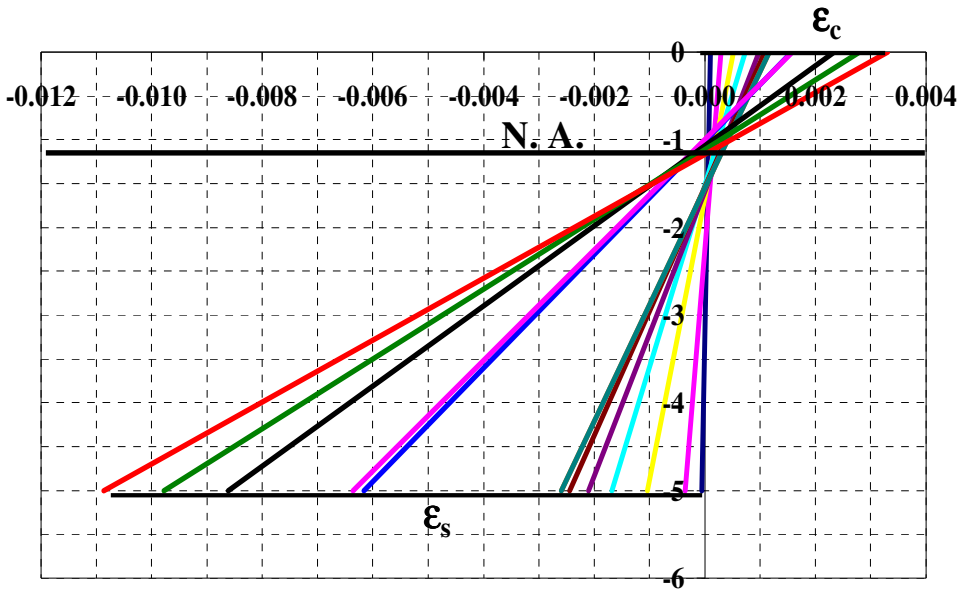

Figure 4.19 – Variation of the depth to the neutral axis with increasing applied moment: linear strain distribution between the concrete and the steel bars

The experimental data show that there is a significant slip between the FRP and steel reinforcement, so that the analytical calculation of the neutral axis is not correct. Because of the slip, the strain level in the FRP laminate cannot be estimated by using the plane section assumption, and the slip effect has to be taken into account.

Figures 4.22 and 4.23 depict the analytical and experimental moments for slab MF-1-L as a function of the experimental steel and FRP strain, respectively. The analytical moment values have been back-calculated using the FRP and steel data collected during the test. The comparison was investigated in order to check the consistency of the experimental strain data that are used in the calculation of the analytical moment. Since there is a good agreement between experimental and analytical moments, it can be confirmed that, due to the significant discrepancy between experimental FRP and steel strains, the conservation of plane section assumption is not acceptable.

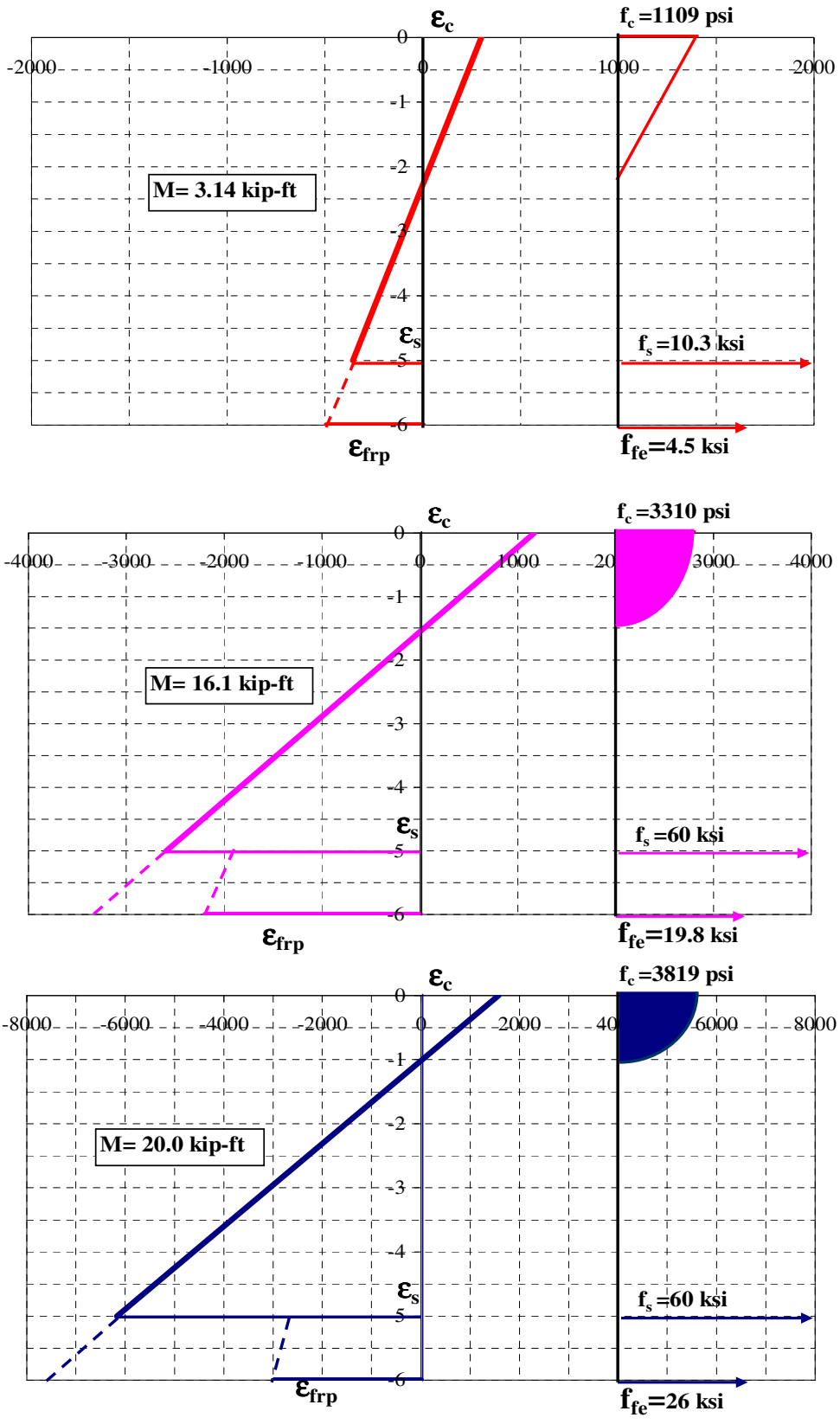

Figure 4.20 – Strain and stress diagrams at midspan for slab MF-1-L

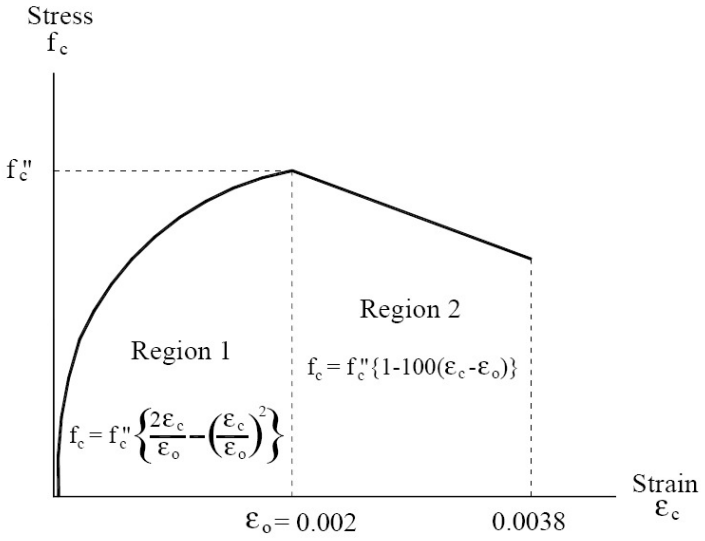

Figure 4.21 – Concrete stress-strain behavior developed by Park and Paulay (1975)

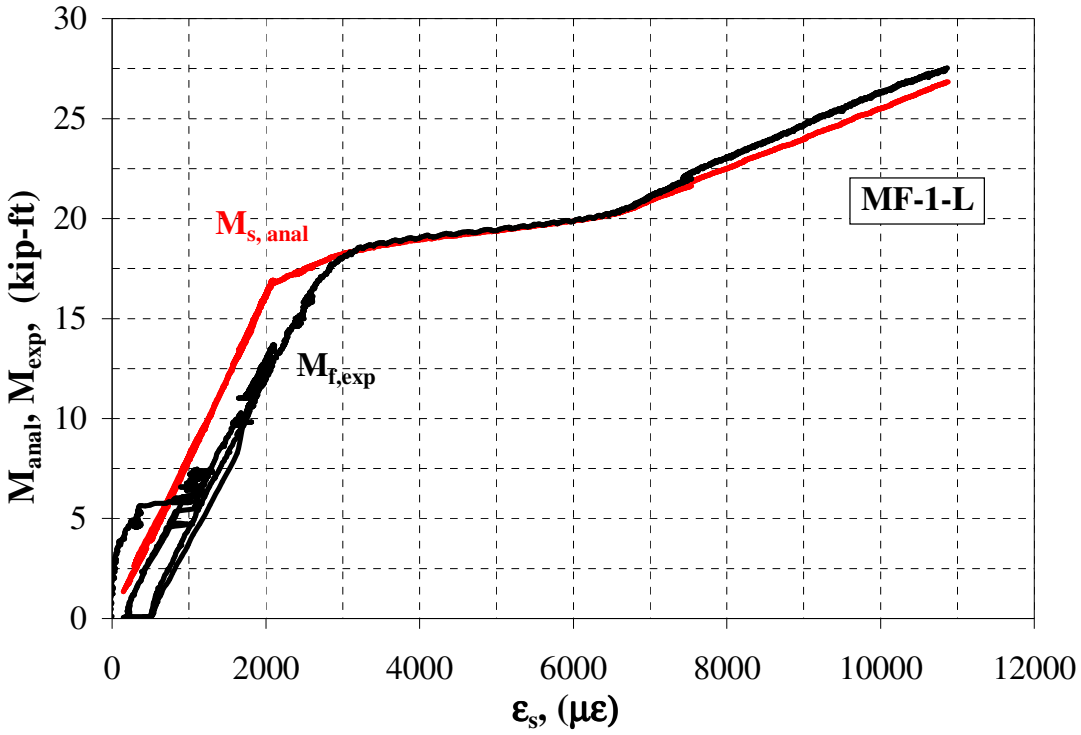

Figure 4.22 – Analytical and experimental moments vs experimental steel strain

(1 kip-ft = 1.356 kN m)

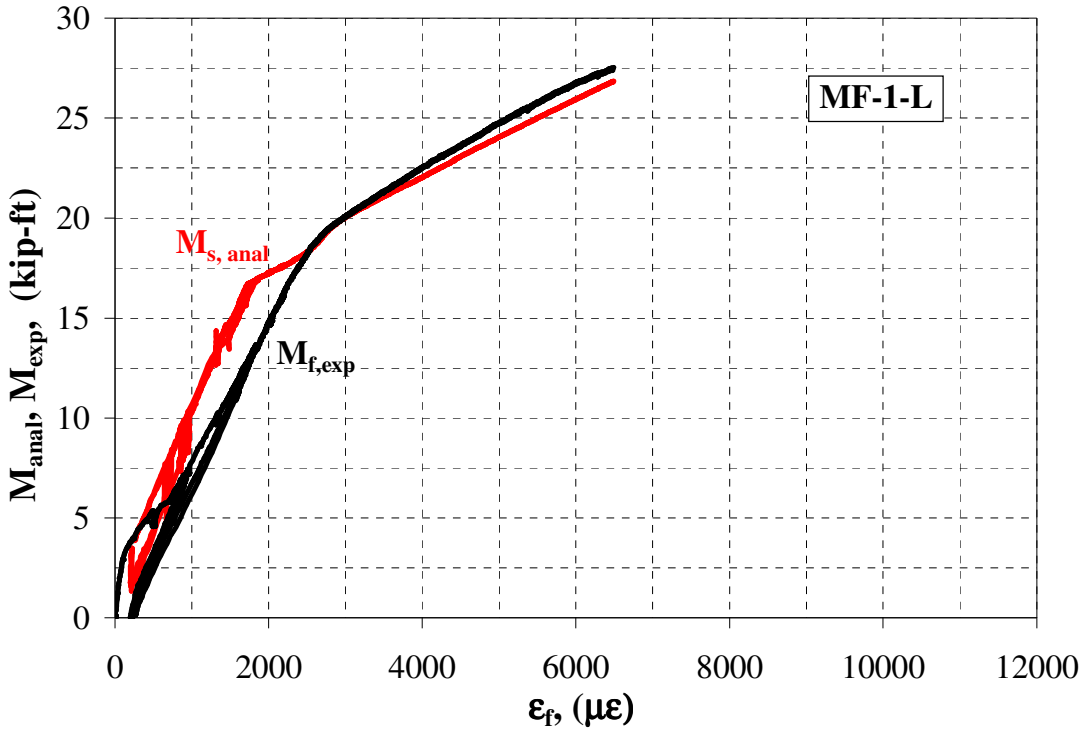

Figure 4.23 – Analytical and experimental moments vs experimental FRP strain

(1 kip-ft = 1.356 kN m)

CHAPTER 5

CONCLUSIONS

In this research project, the experimental behavior of RC one-way slabs strengthened in flexure with MF-FRP laminates has been investigated. The experimental program consisted of four slabs strengthened with a MF-FRP laminate, a counterpart strengthened with a EB-FRP laminate, and a control specimen. The main investigated parameters were the length of MF-FRP laminate and the fastener layout.

Tests results showed that members strengthened with the MF-FRP system exhibited increases in the yielding moment over the control specimen ranging from 15.4 to 23.1%, and increases in the ultimate moment ranging from 30.9 to 58.6%. The flexural strength is comparable to that attained with the EB-FRP system.

The comparison among the experimental curves of MF-FRP strengthened members showed that: 1) spacing of fasteners and length of the FRP laminate play a critical role in the performance of the system; 2) an appropriate combination of these two parameters allows for increasing the deformability of the system without significantly affecting the performance in terms of strength.

A correlation between the number of fastener and the post-yielding deformability of the strengthening system was found. The smaller the number of fasteners used in the system, the greater the ductility and the smaller the stiffness; conversely, the systems were stiffer when larger numbers of fastener were used, but failed at a much smaller displacement.

The experimental-analytical comparison prompted issues related to the use of existing strength models that do not account for the slip occurring between the FRP laminate and the concrete. Due to this phenomenon, the computation of the depth to the neutral axis and of the effective strain in the FRP laminate is not viable by assuming a linear strain distribution between the concrete in compression and the FRP.

CHAPTER 6

RESEARCH NEEDS

6.1 GENERAL

The research project presented in this thesis has investigated the flexural behavior of RC members strengthened with MF-FRP systems. Based on the experimental evidence, the main research needs in this area for the immediate future are outlined as follows.

6.2 DESIGN CONSIDERATIONS

6.2.1 Slip between FRP laminate and concrete

A better understanding of the slip occurring between FRP laminate and concrete is needed. As shown by experimental evidence, the plane section assumption adopted by existing models for MF-FRP systems is not accurate due to the relative deformation between the concrete and the external FRP reinforcement. The slip between the FRP and concrete is induced by the presence of gaps in the connection components, elastic deformation of the bolts and bearing mechanism at the hole locations.

The analysis of test results shows that that the slip plays an important role in determining the effective strain level in the FRP and the depth to the neutral axis. Consequently, more accurate design procedures may be required in order to account for the occurrence of slip. Preliminary studies were performed by Lee et al. (2007) in order to address this issue. They attempted to estimate the nominal moment of MF-FRP strengthened members by introducing a reduction factor for the FRP strain. This factor was defined as the percent difference between the calculated FRP strain based on the fully bonded assumption and the experimentally obtained FRP strain at concrete crushing on top of MF-FRP member. However, this assumption may still be simplistic. In fact, it

has been demonstrated that the depth of the neutral axis should be calculated assuming a strain linear distribution between the concrete in compression and the tensile steel. In addition, more work is needed to quantify the slip between FRP and concrete depending on relevant parameter of the MF connection, such as fastener type and fastener layout.

Characterization of the slip is primarily required in order to address the serviceability limit state. Without understanding the behavior of MF-FRP members at service, this strengthening technique cannot be considered. According to ACI 440.2R-08, the serviceability of a member (deflections and crack widths) under service loads should satisfy the provisions of ACI 318-07. The effect of the FRP external reinforcement on the serviceability can be assessed using the transformed-section analysis. The issue still lies in estimating the effective level of FRP strain if the plane section is not maintained. To avoid inelastic deformations of members under service load levels, the limitations of stresses in the steel reinforcement and in the concrete assumed for EB-FRP strengthened members may be considered. The same criteria can be used for the limitation of stress in the FRP for which a linear-elastic analysis is required. The characterization of the slip becomes a critical issue for addressing the serviceability limit state.

6.2.2 Behavior of MF-FRP connection

For convenience of calculations, the strength models available in the technical literature assume that there is a uniform distribution of load in the fastened FRP laminate. The assumption implies that the force from the FRP laminate at any section is distributed uniformly to the fasteners at that section. Conversely, this assumption implies the force transferred to the FRP strip is directly proportional to the number of fasteners available at the section. Although this approach at ultimate conditions may be acceptable, a more

rigorous approach may be considered. For example, the method of finite differences may be implemented, where the shear force at each fastener is explicitly computed at ultimate on the basis of equilibrium conditions at any section.

6.3 STRUCTURAL PERFORMANCE

Further experimental work is needed to optimize the design of the MF-FRP system: the optimization should focus on the reduction of FRP laminate length (to reduce material cost) and the use of minimum number of fasteners (to enhance constructability). For this purpose, flexural tests on members for which the full utilization of the laminate is attained past yielding of the steel should be considered.

In addition, research is needed to determine the long-term durability of the MF-FRP system. Potential degradation of the strip at the holes should be investigated.

REFERENCES

American Concrete Institute (ACI 2008a), "Guide for the Design and Construction of Externally Bonded FRP Systems for Strengthening Concrete Structures," *ACI 440.2R-08*, ACI Committee 440, Farmington Hills, MI.

American Concrete Institute (ACI 2008b), "Building Code Requirements for Reinforced Concrete and Commentary", *ACI 318R-08*, ACI Committee 318, Farmington Hills, Michigan.

Arora, D., "Rapid Strengthening of Reinforced Concrete Bridge with Mechanically Fastened Fiber-Reinforced Polymer Strips," *M.Sc. Thesis*, University of Wisconsin – Madison, 2003, 353 pp.

Bakis, C. E., Bank, L. C., Brown, V. L., Cosenza, E., Davalos, J. F., Lesko, J. J, Machida, A., Rizkalla, S. H., and Triantafillou, T. C., "Fiber-Reinforced Polymer Composites for Construction- State-of-the-Art Review," *Journal of Composites for Construction*, V. 6, No. 2, 2002, pp. 73-87.

Bank, L.C., Oliva, M.G., Arora D., and Borowicz D. T., "Rapid Strengthening of Reinforced Concrete Bridges," *Report WHRP 03-06*, Wisconsin Highway Research Program, 2003, 166 pp.

Bank, L. C, Borowicz, D. T, Lamanna A. J. , Ray J. C., Velazquez G. I., "Rapid Strengthening of Full-Size Reinforced Concrete Beams with Powder-Actuated Fastening Systems and Fiber-Reinforced Polymer (FRP) Composite Materials," US Army Corps of Engineers, *Report Number ERDC/GSL TR-02-12*, 2002, 110 pp.

Bank, L. C., "Mechanically-Fastened FRP (MF-FRP) – A Viable Alternative for Strenghening RC Members," *Proceedings of CICE 2004*, Adelaide, Australia, 2004, 12 pp.

Bank, L. C., and Arora, D., "Analysis of RC beams Strengthened with Mechanically Fastened FRP (MF-FRP) Strips," *Composite Structures*, V. 79, 2007, pp. 180-191.

BASF,MBRACECF130http://www.basfcc.com.sg/en/products/ConcreteRepairandProtectionSystems/MBrace/MBraceCF130/Documents/MBRACE%20CF130_PDS.pdf, 2008

Camanho, P. P., and Matthews, F. L., "Stress Analysis and Strength Prediction of Mechanically Fastened Joints in FRP: a Review," *Composites Part A*, V. 28, 1997, pp.529-547.

De Lorenzis, L., and Nanni, A., "Characterization of FRP Rods as Near-Surface Mounted Reinforcement," *Journal of Composites for Construction*, V. 5, No.2, 2001, pp. 114-121.

De Lorenzis, L., and Teng, J. G., "Near Surface Mounted FRP Reinforcement: An Emerging Technique for Strengthening Structures," *Composites Part B*, V. 38, 2007, pp.119-143.

Dempsey, D. D., and Scott, D. W., "Wood Members Strengthened with Mechanically Fastened FRP Strips," *Journal of Composites for Construction*, V. 10, No. 5, 2006, pp. 392-398.

Hag-Elsafi, O., Alampalli, S., and Kunin, J., "Application of FRP Laminates for Strengthening of a Reinforced Concrete T-beam Bridge Structure," *Composite Structures*, V. 52, No. 3, 2001, pp. 453–466.

Hassan, N. K., Mohamedien, M. A., and Rizkalla, S. H., "Multibolted Joints for GFRP Structural Members," *Journal of Composites for Construction*, V. 1, No. 1, 1997a, pp. 3-9.

Hassan, N. K., Mohamedien, M. A., and Rizkalla, S. H., "Rational Model for Multibolted Connections for GFRP Members," *Journal of Composites for Construction*, V. 2, No. 1, 1997b, pp. 71-78.

Lamanna, A. J., "Flexural Strengthening of Reinforced Concrete Beams with Mechanically Fastened Fiber Reinforced Polymer Strips," *PhD Thesis*, University of Wisconsin–Madison, 2002, 287 pp.

Lamanna, A. J., Bank, L. C., and Scott, D. W., "Flexural Strengthening of Reinforced Concrete Beams Using Fasteners and Fiber Reinforced Polymer Strips," *ACI Structural Journal*, V. 98, No.3, 2001, pp. 368–376.

Lamanna, A. J., Bank, L. C., and Borowicz, D. T., "Mechanically Fastened FRP Strengthening of Large Scale RC Bridge T Beams," *Advances in Structural Engineering*, V. 7, No. 6, 2004, pp. 525-538.

Lamanna, A. J., Bank, L. C., and Scott, D. W., "Flexural Strengthening of Reinforced Concrete Beams by Mechanically Attaching Fiber-Reinforced Polymer Strips," *Journal of Composites for Construction*, V.8, No. 3, 2004, pp. 203–210.

Lee, J. H, Lopez, M. M., and Bakis, C. E., "Flexural Behavior of Reinforced Concrete Beams Strengthened with Mechanically Fastened FRP Strip," *Proceedings of FRPRCS-8*, University of Patras, Patras, Greece, July 16-18, 2007.

Martin, J. A., and Lamanna, A. J., "Performance of Mechanically Fastened FRP Strengthened Concrete Beams in Flexure," *Journal of Composites for Construction*, V. 12, No. 3, 2008, pp. 257-265.

Powers Fasteners, "Powers Wedge Bolt Specification and Design Manual," Powers Mechanical Anchors and Fasteners Catalogue, 2008.

Quattlebaum, J. B., Harries, K. A., and Petrou, M. F., "Comparison of Three Flexural Retrofit Systems under Monotonic and Fatigue Loads," *Journal of Bridge Engineering*, V. 10, No. 6, 2005, pp. 731-740.

Rizzo, A., "Application of Mechanically Fastened FRP (MF-FRP) Pre-cured Laminates in Off- System Bridges," *M.Sc. Thesis*, University of Missuri-Rolla, 2005, 285 pp.

Rizzo, A., Galati, N., Nanni, A., and Dharani, L.R., "Material Characterization of FRP Pre-Cured Laminates Used in the Mechanically Fastened FRP Strengthening of RC Structures," *SP-230: 7th International Symposium on Fiber-Reinforced (FRP) Polymer Reinforcement for Concrete Structures*," American Concrete Institute, V. 230, pp.135-152.

Rizzo, A., Galati, N., Nanni, A., and Bank, L.C., "Strengthening Concrete Structures with Mechanically Fastened Pultruded Strips," *COMPOSITES 2005*, Columbus, Ohio USA, 2005b, 15 pp.

Rosner, C. N., and Rizkalla, S. H. , "Bolted Connections for Fiber Reinforced Composite Structural Members: Experimental program," *Journal of Materials in Civil Engineering*, V. 7, No. 4, 1995, pp. 223-231.

Spadea, G., Bencardino, F., and Swamy, R. N., "Structural Behavior of Composites RC Beams with Externally Bonded CFRP," *Journal of Composites for Construction*, V. 2, No. 3, 1998, pp. 132-136.

Stallings, J. M., Tedesco, J. W., El-Mihilmy, M., and McCauley, M., "Field Performance of FRP Bridge Repairs," *Journal of Bridge Engineering*, Vol. 5, No. 2, 2000, pp. 107-113.

Strongwell, website: http://www.strongwell.com, 2008

Teng, J. G., Chen, J.F., Smith, S.T., and Lam, L., "FRP-strengthened RC structures," *John Wiley & Sons*, 2002, UK, 245 pp.

Triantafillou, T., and Matthys, S., "Flexural Strengthening with Externally Bonded FRP Reinforcement," *Proceedings of the International Workshop on Composites in Construction: A reality*," 2001, pp. 194-202.

APPENDIX

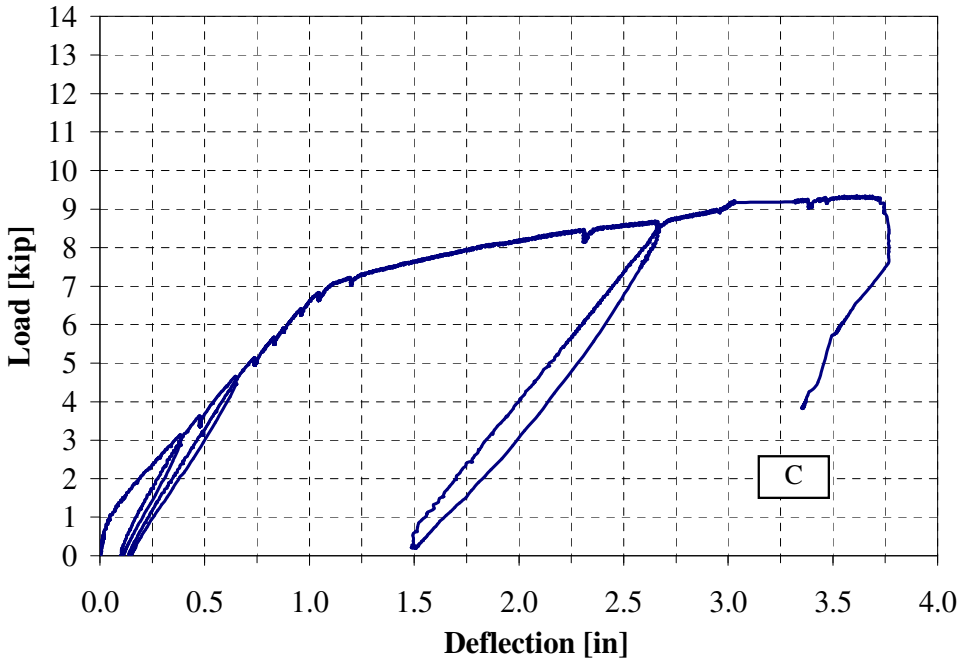

Figure A1 – Load-deflection curve at midspan: slab C

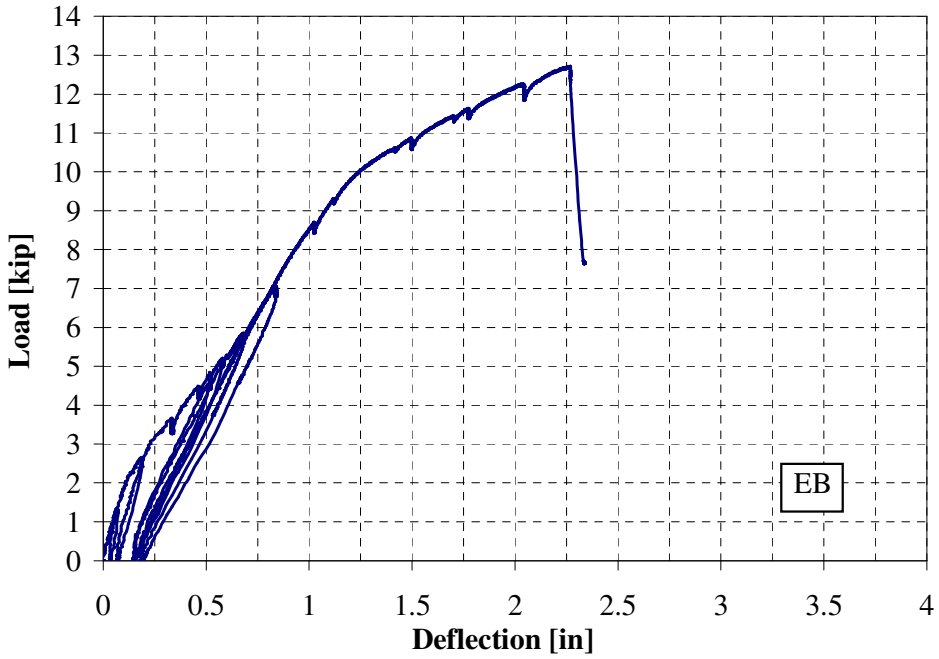

Figure A2 – Load-deflection curve at midspan: slab EB

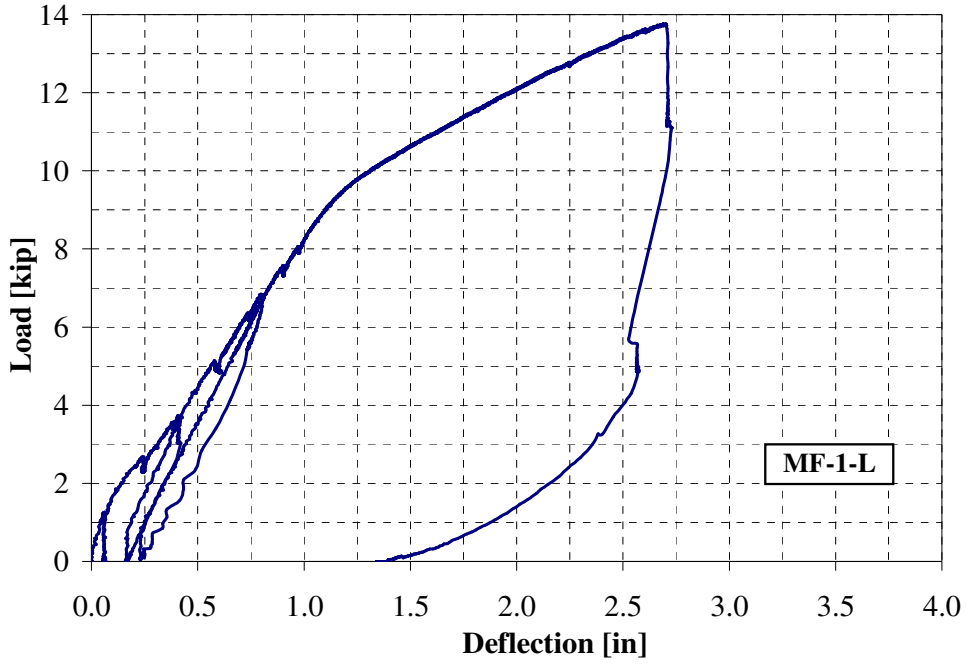

Figure A3 – Load-deflection curve at midspan: slab MF-1-L

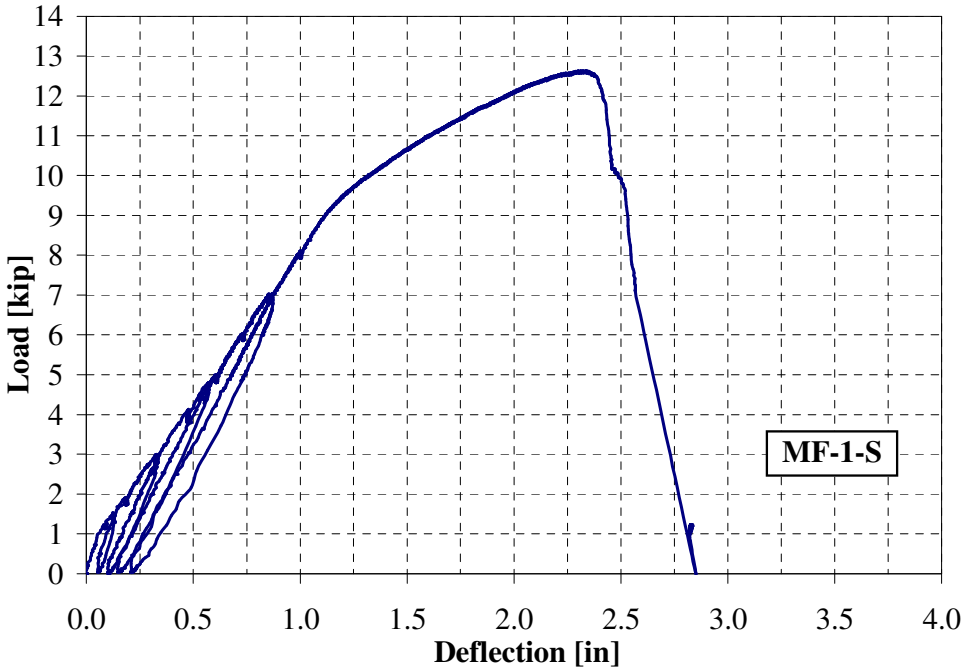

Figure A4 – Load-deflection curve at midspan: slab MF-1-S

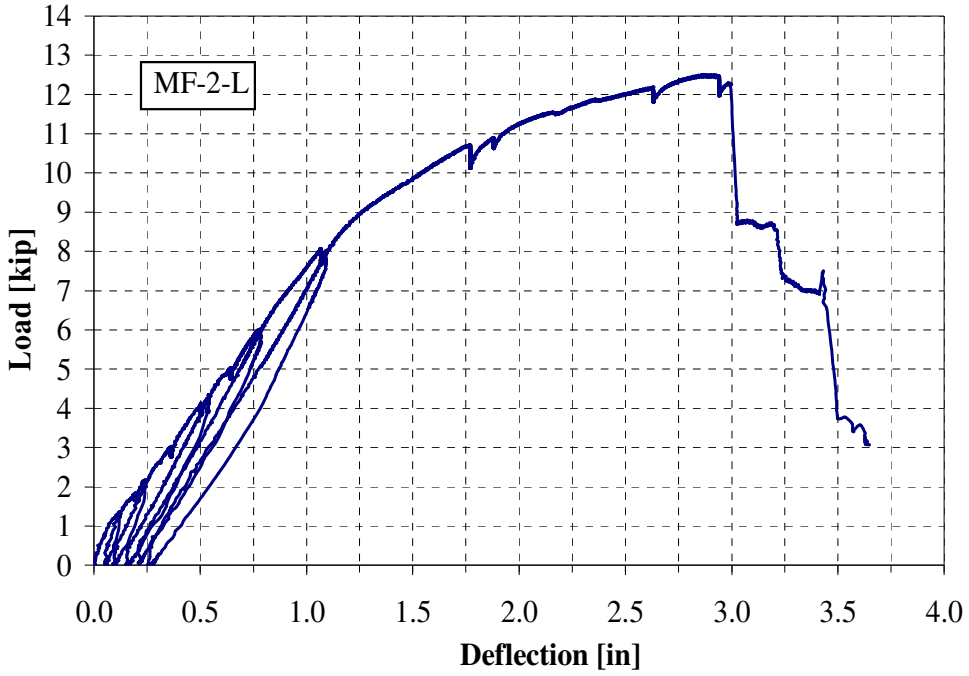

Figure A5 – Load-deflection curve at midspan: slab MF-2-L

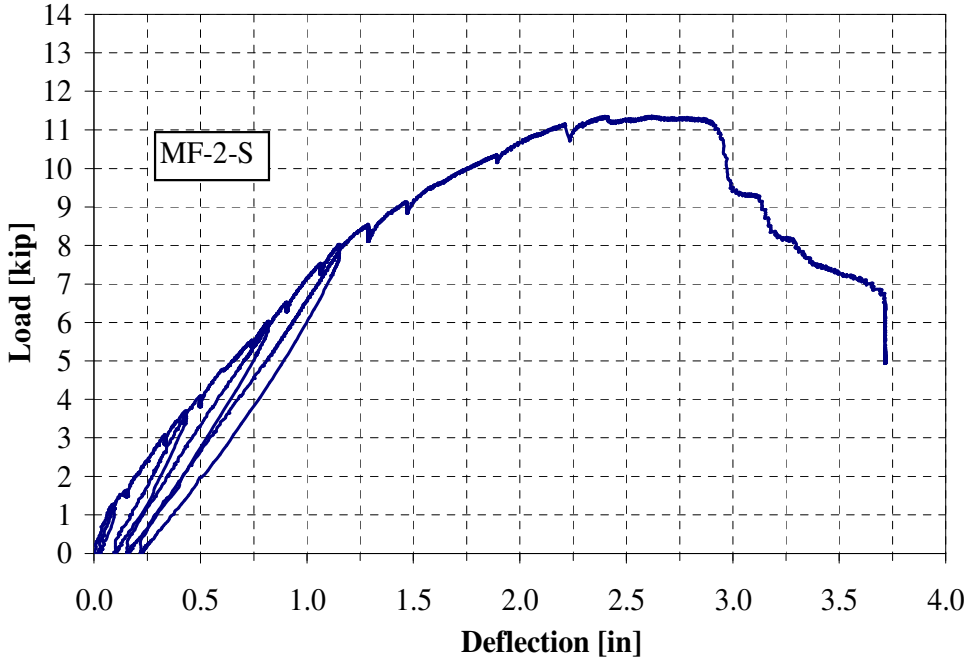

Figure A6 – Load-deflection curve at midspan: slab MF-2-S

(1 kip = 4.45 kN; 1 in =25.5 mm)